Final Draft
of the original manuscript:

Rheology in shear and elongation and dielectric spectroscopy of polystyrene-*block*-poly(4-vinylpyridine) diblock copolymers

Tarek Kollmetz, Prokopios Georgopanos, and Ulrich A. Handge*

*Helmholtz-Zentrum Geesthacht, Institute of Polymer Research,
Max-Planck-Strasse 1, 21502 Geesthacht, Germany*

ABSTRACT

We elucidate the influence of composition (weight ratios of 89/11, 76/24 and 49/51) and morphology (spherical, cylindrical and lamellar) on the dielectric and viscoelastic properties in shear and elongation of anionically synthesized polystyrene-*block*-poly(4-vinylpyridine) (PS-*b*-P4VP) diblock copolymers in the microphase-separated state. The temperature dependence of the response in both experiments is compared. The analysis of the linear regime shows the appearance of composition (superposition of moduli) and interfacial effects caused by microphase separation (low frequency shoulder, plateau and $\omega^{1/2}$ regime for dynamic moduli and Maxwell-Wagner-Sillars polarization in dielectric experiments). In shear and extensional flows with a constant deformation rate, a pronounced strain-softening behavior in case of a cylindrical and a lamellar morphology appears. For a high weight fraction of the majority phase and a spherical morphology, respectively, strain-softening is observed to a lesser extent. Consequently, strain-softening of diblock copolymer melts can be tuned by the weight/volume ratio of the two blocks.

*E-mail: ulrich.handge@hzg.de

1

1. Introduction

The influence of molecular structure on the macroscopic properties of polymers is a key research topic of modern polymer science. In comparison to homopolymers, the static and dynamic properties of block copolymers are associated with additional phenomena, e.g., microphase separation.[1-3] This phenomenon can be used for further applications such as nanostructuring[4] and membrane preparation[5, 6] because of the rich variety of block copolymer microstructures on the nanometer scale.[7] Furthermore, processing of polymers is intimately associated with the rheological properties in the melt state or in solution. For example, preparation of polymer films using the technique of film blowing requires polymers which show strain-hardening in melt elongation in order to achieve films with a uniform thickness. Driven by high technological relevance and fundamental interest, a variety of chemically and rheologically oriented studies thus revealed the influence of long-chain branching of polyolefins on the rheological properties in melt elongation.[8-13] On the contrary, if a polymer depicts strain-softening in melt elongation, it may be advantageous for preparation of open-celled foams. During expansion of foam cells, a biaxial elongational flow in the polymer matrix exists. The strain-softening property of the polymer favors break-up of the cell walls during foaming. In previous publications, such a strain-softening behavior was observed for some selected block copolymers with a cylindrical structure, e.g., for a polystyrene-*block*-poly(4-vinylpyridine) (PS-*b*-P4VP) diblock copolymer with a cylindrical morphology.[14, 15] Therefore microphase-separated block copolymers can have a high impact for preparation of open-celled polymer foams. However, a systematic analysis of the strain-softening potential of diblock copolymers is still missing, in particular for different types of block copolymer morphologies.

A series of theoretical and experimental publications has been devoted to the static[16, 17] and dynamic properties of block copolymers,[2, 18-22] for example, in order to analyze the influence of the molecular weight,[23] the composition[24] and, in case of triblock copolymers, the block sequence[25] on the rheological properties. Recently, bottlebrush block copolymers were also studied which were characterized by a high mobility and a fast ordering dynamics because of the low molecular weight side chains.[26] In this work, we focus on PS-*b*-P4VP diblock copolymers because of the high value of Flory-Huggins interaction parameter χ for the pair styrene/4-vinylpyridine. Furthermore, in contrast to the intensively studied polystyrene-polyisoprene (PS-*b*-PI) block copolymers, the glass transition temperature T_g of the P4VP component is larger than the T_g value of polystyrene, and the difference of T_g values for P4VP and PS is significantly smaller than for PS and PI. In the previous works, the viscoelastic and dielectric properties of polystyrene-*block*-poly(2-vinylpyridine) (PS-*b*-P2VP) and polystyrene-*block*-poly(4-vinylpyridine) block copolymers were studied.[27-29] Schulz et

al. determined the phase behavior of PS-*b*-P2VP diblock copolymers with various compositions using rheological and scattering techniques as well as transmission electron microscopy.[30] The volume fraction of the PS microphase ranged between 34 and 70%, and the number average of the molecular weight was below 20 kg/mol. The rheological experiments of Schulz et al. were performed in the linear regime. Fang et al. analyzed the influence of molecular weight on the rheological properties of PS-*b*-P2VP diblock copolymers with a lamellar morphology.[31] The dynamic moduli G' and G'' follow a power law relation as a function of angular frequency ω with a power-law exponent in the order of 0.5. This value of the power law exponent was also theoretically derived by Kawasaki and Onuki.[32] The orientation of lamellae by large amplitude oscillatory shear flow and the localization of functionalized multi-wall carbon nanotubes in a PS-*b*-P4VP diblock copolymer was thoroughly studied by Wode et al.[33]

The rheological properties of poly(2-vinylpyridine) homopolymers were also the subject of several publications. The influence of nanoparticle loading on the relaxation behavior of poly(2-vinylpyridine) was studied by Holt et al.[34] A main result of their work is that the addition of nanoparticles does not slow down the overall chain dynamics. For example, the glass transition temperature was not altered by the addition of the particles, compare also the results of Handge et al.[35] The experiments of Takahashi et al. show that poly(2-vinylpyridine) and polystyrene (PS) have a similar zero shear rate viscosity η_0 whereas the plateau modulus G_N^o and the elastic creep compliance J_e^o of P2VP and PS slightly differ.[36]

Besides a large number of studies on the rheological properties of block copolymer melts in shear flow, only a limited number has been devoted to the extensional rheology of microphase-separated block copolymers. Takahashi et al. concluded that strain-softening and strain-hardening of random and block copolymers is associated with the damping function.[37] In recent works, the morphology development of block copolymers with a cylindrical morphology using scattering techniques was studied.[38-40] The initial orientation of the triblock copolymer had a strong influence on the flow kinematics leading to a uniaxial deformation for cylinders which are aligned in parallel to the flow direction and to a planar deformation for perpendicularly aligned samples. The relaxation behavior was also studied in detail. If the Hencky strain in the elongation interval exceeded a certain critical value, stress relaxation took place faster than for an elongation up to a Hencky strain below this critical value.[40]

Broadband dielectric spectroscopy is a further tool to study the dynamical properties of polymers.[41] This method can give much insight into the relaxation behavior of the different blocks of block copolymers and on interfacial relaxation. Several studies were devoted to the dielectric properties of PS-*b*-P2VP and PS-*b*-P4VP diblock copolymers and the corresponding homopolymers. The segmental dynamics of P2VP

3

homopolymers in nanopores were investigated by Serghei.[29] The α-relaxation of P2VP did not significantly change down to a pore diameter of 18 nm. In a similar manner, it was shown that the glass transition temperature of a PS-*b*-P4VP diblock copolymer with a symmetric composition was not altered, either, during capillary flow into nanowires.[29] The dielectric properties of a PS-*b*-P4VP diblock copolymer with a cylindrical morphology in the bulk and confined in cylindrical nanopores were studied by Maiz et al.[42] In a confined geometry, a faster dynamics is observed. A major outcome of the work of Sanno et al. is that the β-relaxation process of isotactic and atactic poly(2-vinylpyridine)s can be attributed to the restricted rotation of pendant pyridine rings accompanying a distortion of the main chains.[43] The glass transition temperature of thin and ultrathin P2VP films was measured by Madkour et al.[44] The authors did not find a shift of glass transition temperature down to a film thickness of 22 nm, either.

The objective of this study is to analyze the influence of composition and different types of morphology on the rheological and dielectric properties of polystyrene-*block*-poly(4-vinylpyridine) diblock copolymers and to compare the temperature dependence of selected relaxation processes in both experiments. Several diblock copolymers with varying composition and molecular weight were synthesized. Rheological experiments in shear and elongation were performed and analyzed in order to elucidate the linear and nonlinear material behavior. In addition, dielectric spectroscopic measurements were carried out in order to achieve an almost complete view of the relaxation behavior of these polymers. In contrast to previous studies, different types of microphase-separated morphology are investigated in this work.

2. Experimental section

2.1. Materials

Styrene ($\leq$99.5%, Sigma-Aldrich, Schnelldorf, Germany) was filtered through a chromatography column filled with aluminum oxide powder (Al_2O_3, Macherey-Nagel, Düren, Germany) in order to remove inhibitor and was transferred to a glass flask containing di-*n*-butylmagnesium (1.0 M solution in heptane, Sigma-Aldrich, Schnelldorf) under argon. Styrene was distilled before use under high vacuum. 4-vinylpyridine (100 ppm hydroquinone as inhibitor, Sigma-Aldrich, Schnelldorf) was purified from aluminum oxide column. Then 4-vinylpyridine was distilled through a special glass column under distillation apparatus at a reduced pressure of approximately 40 mbar at 95 °C and was subsequently transferred to a glass flask and stirred over calcium hydride (99%, Sigma-Aldrich, Schnelldorf). The next step was the purification and distillation (twice) from ethylaluminum dichloride (1.0 M in hexane, Sigma-Aldrich, Schnelldorf). Tetrahydrofuran (THF, $\leq$99.9%, Merck, Darmstadt,

4

Germany) was used as a solvent. It was successively distilled from molecular sieves and titrated with *sec*-butyllithium (*s*-BuLi, 1.4 M in hexane, Sigma-Aldrich, Schnelldorf) obtaining a yellow color. For the polymerization, *s*-BuLi was used as initiator. For the termination, a 10:1 v/v mixture of methanol (99.8%, Sigma-Aldrich, Schnelldorf) and acetic acid (99.7%, Sigma-Aldrich, Schnelldorf) was used as termination agent.
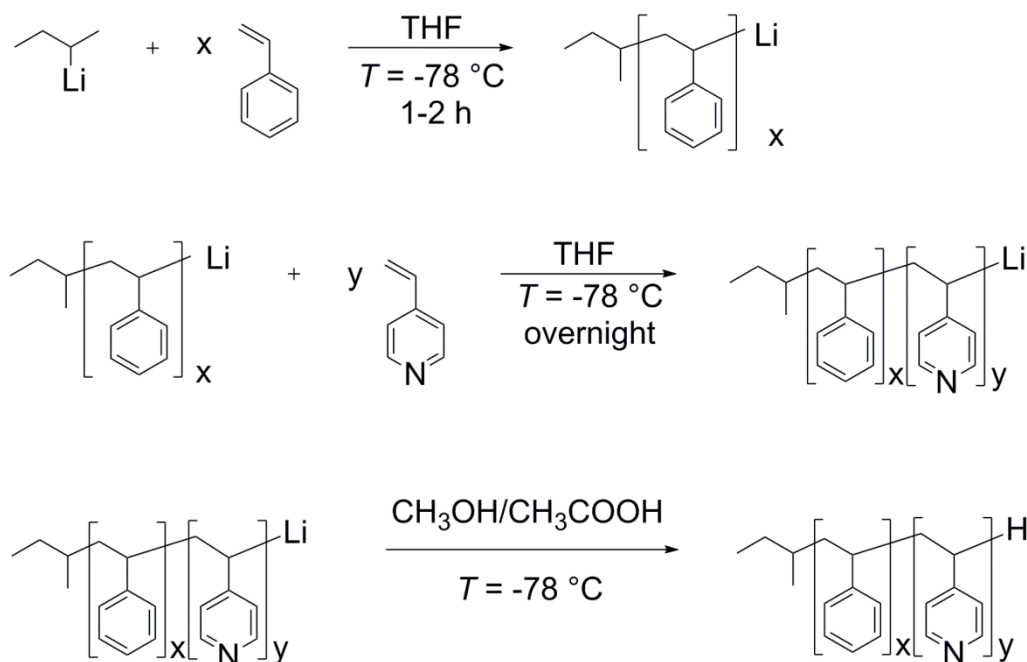
Scheme 1: Synthesis of polystyrene-*block*-poly(4-vinylpyridine) (PS-*b*-P4VP) diblock copolymers.

2.2. Synthesis

The polystyrene-*block*-poly(4-vinylpyridine) (PS-*b*-P4VP) diblock copolymers were synthesized via sequential anionic polymerization. The day before the start of the synthesis the solvent was distilled from *s*-BuLi and was titrated until the yellow color of the solution remained stable for approximately 15 min at -20 °C. Afterwards, the solution was heated up to room temperature so that the color vanished and finally was evacuated.

The polymerization process is displayed in Scheme 1. The polymerization of styrene was carried out at -78 °C for approximately 1 – 2 hours. Initially, the distilled styrene was added with a syringe over argon into the polymerization flask. After polymerization initiation with *s*-BuLi, the solution obtained an orange color which is characteristic of the active living ends of the polystyrene chains. After a polymerization time of 1 – 2 hours, a small aliquot of the solution was extracted for characterization, while the distilled 4-vinylpyridine monomer was also added to the solution and left to polymerize overnight at -78 °C. The polymerization solution obtained a stronger yellow color

5

indicating the addition of the monomeric unit of P4VP on the polymer chain. On the following day, the polymerization was terminated by insertion of a small amount of a degassed methanol/acetic acid mixture into the polymerization solution. Then the solution was left to equilibrate to room temperature by rigorous stirring, and the excess of the solvent was removed by rotational evaporation at 60 °C. The synthesized diblock copolymers were precipitated in water and dried under vacuum at 60 °C for several days. For the polymers, the nomenclature PS_x-b-$P4VP_y^z$ is used, where x and y are the weight fractions of PS and P4VP, respectively, and z is the total molecular weight of the diblock copolymer in kg/mol.

The synthesis of the diblock copolymers was focused on producing polymers with a ratio of PS/P4VP approximately equal to 90/10, 75/25 and 50/50 in order to achieve different microphase-separated morphologies. However, since tetrahydrofuran is not a good solvent for P4VP, the increase of the molecular weight of P4VP led to partial solubility problems, which were indicated by an observed turbidity in the polymerization solution. This was an indication of the increased molecular weight of the P4VP chains that led to the partial insolubility of the polymer. For comparison a commercial P4VP homopolymer (Polymer Source Inc., Dorval, Canada) with a number average of the molecular weight of 42 kg/mol and a polydispersity index of 1.45 was used for experimental analysis. As a further reference, a commercial polystyrene PS 158K (BASF SE, Ludwigshafen, Germany) with a number average molecular weight of 113 kg/mol and a polydispersity index of 2.3 was used.[15]

2.3. Molecular and thermal characterization

The diblock copolymers were characterized by several analytic methods in order to obtain information about the molecular weight distribution and the molecular structure of the diblock copolymers. Molecular characterization was accomplished with the use of gel permeation chromatography (GPC) in order to obtain the polydispersity index and the molecular weight of the synthesized polymer as well as proton nuclear magnetic resonance (^{1}H-NMR). GPC measurements were performed at room temperature in THF on a Waters instrument (Waters GmbH, Eschborn, Germany). The GPC system was equipped with polystyrene gel columns of 10, 10^2, 10^3, 10^4 and 10^5 Å pore sizes and a refractive index (RI) detector. The GPC device was calibrated with polystyrene standards of different molecular weights (PSS Polymer Standards Service GmbH, Mainz, Germany). ^{1}H-NMR was accomplished with the Avance 500 spectrometer (Bruker BioSpin GmbH, Rheinstetten, Germany), equipped with a 500 MHz magnet and a triple resonance inverse (TXI) probe. The experiment was done at room temperature with deuterated chloroform as solvent and tetramethylsilane as internal standard.

Thermogravimetric analysis (TGA) was carried out using the apparatus TG 209 F1 Iris (Netzsch, Selb, Germany). The experiments were done in a temperature range from 25 °C up to 1000 °C at a heating rate of 10 K/min. The measurements were performed under an argon atmosphere. TGA-FTIR experiments were carried out using the apparatus TGA/DSC2 Star (Mettler-Toledo, Gießen, Germany) coupled with a TGA-IR spectrometer Nicolet iS 50FT-IR (Thermo Scientific, Braunschweig, Germany). Isothermal experiments at temperatures of 140 °C and 270 °C were also carried out.

Differential scanning calorimetry (DSC) experiments were performed with the use of the calorimeter DSC 1 (Mettler-Toledo, Gießen, Germany) in the temperature range from 25 °C up to 250 °C. The heating rate was 10 K/min. The second heating interval was used for the evaluation of the thermal properties. The measurement was performed in a nitrogen atmosphere. Approximately 10 mg of the polymer were placed in an aluminum pan of 10 μL.

2.4. Morphological characterization

The analysis of the morphology was done via transmission electron microscopy (TEM). The samples were obtained from compression-molding as described below and molten in the rheometer for 7 min at 240 °C. Subsequently, a shear deformation or an elongation, respectively, for 10 s was applied with a shear or extension rate (Hencky strain rate) of 0.1 s^{-1}. The samples for the TEM analysis were quenched to room temperature by opening the rheometer after the melting time of 7 min for the samples which are denoted as "prior to deformation." In order to investigate the change of morphology during deformation, additional samples after deformation in shear or extension for 10 s were obtained in the same manner. After quenching, the samples were cut using an ultramicrotome EM UCT (Leica Microsystems, Wetzlar, Germany) into slices with a thickness of approximately 50 nm. The ultrathin cuts were placed on gold coated copper grids and stained with iodine for 1 hour in order to obtain good electron density contrast. A Tecnai G^2 F20 (FEI, Eindhoven, The Netherlands) was used to obtain the TEM micrographs at 120 kV in bright field mode.

2.5. Rheological experiments

Cylindrical specimens with a diameter of 8 mm and a thickness of 1 mm for rheological experiments in shear were prepared by compression-molding. Initially, the bulk polymer powder was dried at 140 °C under vacuum overnight. Then the sample was compression-molded using a laboratory press PW 10 (Paul-Otto Weber GmbH, Remshalden, Germany) at 200 °C for approximately 9 min, applying a force of approximately 60 kN and a vacuum of 10^{-2} mbar. Samples prepared by compression-molding were also used for dynamic-mechanical-thermal analysis (DMTA) under

tension and for melt elongational experiments. The samples for DMTA had rectangular cross-sections with dimensions of approximately 26.0 x 4.5 x 0.25 mm^3 and the samples for extensional rheology 15.0 x 10.0 x 0.75 mm^3. The samples of lower molecular weight, PS$_{74}$-b-P4VP$_{26}$^{79} and PS$_{49}$-b-P4VP$_{51}$^{60}, were prepared by compression moulding with the MeltPrep device (MeltPrep GmbH, Graz, Austria) at 200 °C for 10 min and a pressure of 0.1 bar. After compression-molding the P4VP homopolymer and the PS-b-P4VP diblock copolymers were kept at 140 °C in vacuum for at least 24 hours.

Experiments in the extension mode were performed using the Solids Analyzer RSA II (Rheometrics, Piscataway (NJ), USA) in a nitrogen atmosphere between 25 and 140 °C. The heating rate was 0.5 K/min, and the frequency f was equal to 1 Hz. Before the temperature-dependent experiment, a strain sweep at a temperature of 25 °C in the interval from 0.02 up to 0.2% was carried out in order to determine the linear viscoelastic range. For the temperature sweep experiment, the strain amplitude was set to 0.1%.

The rheological experiments in shear were conducted using the rotational rheometer MCR 502 (Anton Paar, Graz, Austria) in the oscillatory mode and at constant shear rate, respectively. The temperature of the dynamic-mechanical-thermal analysis (temperature sweep) in shear ranged from 240 to 120 °C. The cooling rate was set to -0.5 °C/min, and the shear amplitude γ_0 was 0.5%. The frequency f was equal to 1 Hz. The temperature equilibration time was 7 min.

Furthermore, linear viscoelastic shear oscillations were carried out in the temperature range from 120 to 240 °C in increments of 20 °C. The angular frequency ω was varied between 10^{-2} and 10^2 rad/s, starting from the highest frequency. Strain sweep experiments were carried out before the frequency sweep experiments in order to determine the linear viscoelastic regime. The strain amplitude γ_0 was 5%. In order to probe the stability of the dynamic moduli with time, time sweeps with a constant angular frequency $\omega = 0.10 \ \mathrm{rad}/s$ and a shear amplitude $\gamma_0 = 5\%$ were performed.

The experiments at constant shear rate (so-called stress growth experiments) were conducted with applied shear rates $\dot{\gamma}_0$ of 0.01, 0.10 and 1.00 s^{-1} at a temperature of 240 °C. A plate-plate geometry with a plate diameter of 8 mm was used. The measurements consisted of an interval with constant shear rate of 100 s and a subsequent relaxation interval (shear rate equal to zero) of 100 s.

Rheological experiments in melt elongation were carried out using an SER tool (Anton Paar, Graz, Austria) at a measurement temperature of 180 °C and 240 °C. After the rectangular samples had been attached to the drums, a temperature equilibration time

of 300 s was added. In the temperature equilibration interval, a low pre-torque of 10 μNm was applied according to the method of Aho et al. in order to minimize sagging of the sample.[45] The maximum Hencky strain $\varepsilon_{\max}$ was 4. The Hencky strain rate $\dot{\varepsilon}_0$ was set to 0.01, 0.10 and 1.00 s^{-1}, respectively.

2.6. Broadband dielectric spectroscopy

Dielectric spectroscopy measurements were performed using an Alpha-AN high resolution dielectric analyzer (Novocontrol Technologies GmbH, Montabaur, Germany). Films were obtained from compression-molding powder of the diblock copolymers at 200 °C using the same procedure as the specimens for rheological characterization, which led to films of approximately 180 μm thickness. After compression-molding, the samples were dried at 140 °C under vacuum for at least 24 h. A second gold-coated brass plate was placed on top of the sample. Afterwards, the two gold-coated brass plates containing the sample were inserted in the spectrometer. The diameters of the brass plates were 40 mm for the lower plate and 20 mm for the upper plate. Prior to the dielectric measurements the diblock copolymers were annealed at 200 °C for 1 hour (180 °C for the P4VP homopolymer and 130 °C for the PS homopolymer) in the device in order to improve the contact of the sample with the surface of the electrode. The temperature of the frequency dependent measurements ranged from -50 to 200 °C in increments of 5 °C for the homopolymers and from -50 to 250 °C for the diblock copolymers. The frequency ranged in the interval of 10^{-2} Hz up to 10^7 Hz.

3. Results and discussion

3.1. Molecular characteristics of diblock copolymers

In this work, six PS-*b*-P4VP diblock copolymers with different compositions and molecular weights were synthesized, see Table 1. Referring to the weight fraction of both blocks and the theoretically proposed phase diagram of Bates and Fredrickson,[46] one diblock copolymer is assumed to be associated with a spherical morphology, two diblock copolymers with a cylindrical and three diblock copolymers with a lamellar morphology, respectively.[46] The number average molecular weight M_n varied from 60 kg/mol to 150 kg/mol. The polydispersity index ($Đ$) was small which is characteristic for anionic polymerization. Of special interest is the higher molecular weight diblock copolymer with the symmetrical composition that exhibits a higher polydispersity index than the other diblock copolymers. The reason for this effect is the solubility problem of the synthesized P4VP block during polymerization, since tetrahydrofuran is not a good solvent for P4VP. This explanation is also supported by the fact that the lower molecular weight diblock copolymer with a composition of 50/50 (PS$_{49}$-*b*-P4VP$_{51}^{60}$)

9

Polymer[a]	Φ_{PS}[b] (vol%)	Φ_{P4VP}[b] (vol%)	M_n[c] (g/mol)	Đ[c]
PS$_{89}$-*b*-P4VP$_{11}$^{170}	88.7	11.3	170 000	1.09
PS$_{74}$-*b*-P4VP$_{26}$^{79}	74.0	26.0	79 000	1.20
PS$_{76}$-*b*-P4VP$_{24}$^{159}	76.2	23.8	159 000	1.15
PS$_{49}$-*b*-P4VP$_{51}$^{60}	49.0	51.0	60 000	1.07
PS$_{48}$-*b*-P4VP$_{52}$^{120}	48.0	52.0	120 000	1.31
PS$_{49}$-*b*-P4VP$_{51}$^{131}	49.5	50.5	131 000	1.27

[a] Lower-case numbers indicate the mass fraction of the corresponding block in %. The upper-case number indicates the number average of the molecular weight in kg/mol.

[b] Calculated based on ^{1}H-NMR data.

[c] Determined by GPC calibrated with polystyrene standards and ^{1}H-NMR.

Table 1: Physical properties of the PS-*b*-P4VP diblock copolymers of this study. The volume fractions of the two blocks are denoted by Φ_{PS} and Φ_{P4VP}.

exhibits a lower Đ value than the diblock copolymer PS$_{49}$-*b*-P4VP$_{51}$^{131}.

3.2. Thermal properties of diblock copolymers

Thermal gravimetric analysis (TGA) was applied in order to determine the thermal stability of the diblock copolymers of this study. Figure 1(a) presents the relative mass as a function of temperature for the diblock copolymer PS$_{74}$-*b*-P4VP$_{26}$^{79} and its polystyrene precursor with a number average of the molecular weight M_n of 64 kg/mol. The data for a pristine P4VP with $M_n = 42\,\mathrm{kg/mol}$ are also shown. The comparison of the two curves clearly reveals that the addition of the P4VP block to the polystyrene precursor reduces the thermal stability. Whereas the polystyrene precursor has a mass loss of 1% at a temperature of 374 °C, the corresponding temperature for the PS$_{74}$-*b*-P4VP$_{26}$^{79} diblock copolymer is lower and equals 311 °C. The corresponding value for pristine P4VP is 204 °C. Figure 1(b) presents the derivative of the relative mass as a function of temperature and reveals that the P4VP block and homopolymer are associated with a significant mass loss at lower temperatures than pristine polystyrene. Further TGA measurements revealed that the diblock copolymers are generally stable up to around 300 °C under heating with a rate of 10 K/min.
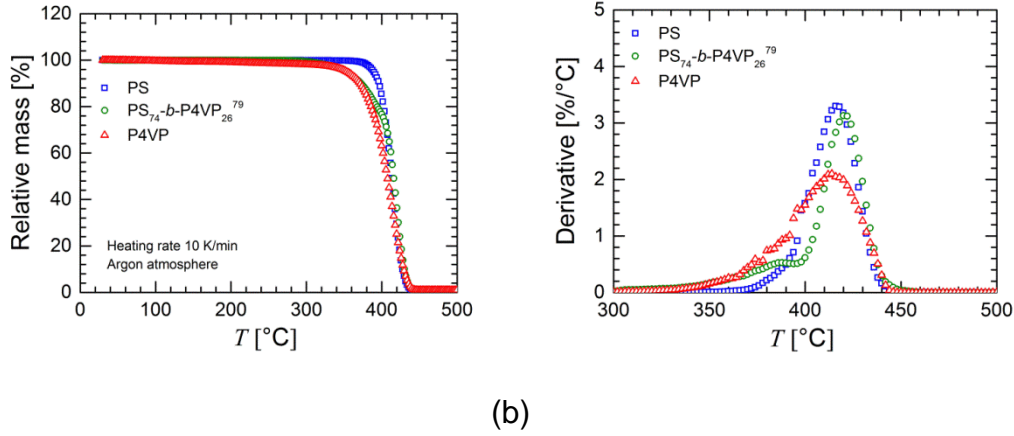
Figure 1: (a) Relative mass and (b) its derivative as a function of temperature as obtained by TGA experiments with a constant heating rate for the diblock copolymer PS$_{74}$-b-P4VP$_{26}$[79], its polystyrene precursor with a number average M_n of the molecular weight of 64 kg/mol and a pristine P4VP with a number average of the molecular weight of 42 kg/mol. The heating rate was 10 K/min.

Polymer	$T_{g, \text{PS Prec}}$ (°C)	$T_{g, \text{PS}}$ (°C)	$T_{g, \text{P4VP}}$ (°C)	$\Delta c_{p, \text{PS}}$ (J/(gK))	$\Delta c_{p, \text{P4VP}}$ (J/(gK))
PS	-	103.7	-	0.230	0
PS$_{89}$-b-P4VP$_{11}$[170]	104.5	104.7	145.2	0.210	0.018
PS$_{74}$-b-P4VP$_{26}$[79]	103.6	105.0	146.0	0.175	0.043
PS$_{76}$-b-P4VP$_{24}$[159]	104.7	105.6	152.8	0.140	0.031
PS$_{49}$-b-P4VP$_{51}$[60]	101.2	102.1	150.0	0.088	0.085
PS$_{48}$-b-P4VP$_{52}$[120]	103.9	104.6	152.5	0.063	0.053
PS$_{49}$-b-P4VP$_{51}$[131]	104.1	104.1	153.0	0.088	0.062
P4VP	-	-	146.9	0	0.220

Table 2: Glass transition temperatures T_g and specific heat capacity Δc_p of pristine polystyrene, poly(4-vinylpyridine) and the PS-b-P4VP diblock copolymers of this study.

The thermal transitions of the diblock copolymers were analyzed using differential scanning calorimetry. The specific heat flux as a function of temperature as determined by the second heating cycle is presented in Figure 2(a). The results of the DSC experiments are also listed in Table 2. The curves are vertically shifted for clarity. Because of the similar weight fraction of the PS and the P4VP blocks, two endothermic processes can be most clearly seen at approximately 105 °C and 150 °C in the thermograph of the PS$_{49}$-b-P4VP$_{51}$[131] diblock copolymer. These two processes correspond to the glass transitions of the PS and the P4VP blocks, respectively. The change of the heat flux at around 105 °C for the diblock copolymers with polystyrene as the majority phase (PS$_{89}$-b-P4VP$_{11}$[170] and PS$_{76}$-b-P4VP$_{24}$[159]) is significantly larger than the one at around 150 °C because of the higher fraction of the PS block in

11

comparison to the lower fraction of the P4VP block. The two distinct endothermic processes at the predicted glass transition temperatures of each block indicate that the microphase-separated diblock copolymers are associated with the strongly segregated regime.

Figure 2(b) displays the measured value of the specific heat capacity Δc_p versus the weight fraction of the PS and the P4VP block. The prediction based on a linear mixing rule and the specific heat capacity of pristine PS and P4VP are also shown. In case of both glass transitions, the measured Δc_p values of the diblock copolymers generally range below the theoretical prediction of the linear mixing rule. This effect can be explained by the contribution of the PS/P4VP interface where the chain segments are less mobile and do not contribute to the Δc_p value.

(a)   (b)
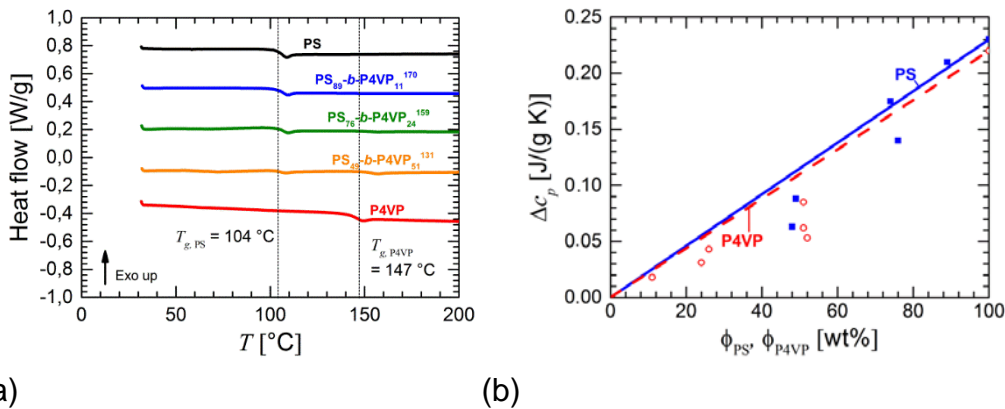
Figure 2: (a) DSC thermograms of PS-*b*-P4VP diblock copolymers of this study with different compositions and a large molecular weight. The heating rate was 10 K/min. For clarity, the curves are shifted vertically. The vertical lines denote the glass transition temperatures of the homopolymers. (b) Specific heat capacity Δc_p as a function of the weight fraction ϕ_{PS} of PS and the weight fraction ϕ_{P4VP} of P4VP, respectively. The circles correspond to ϕ_{P4VP} and the squares to ϕ_{PS}. The result of a linear mixing rule is shown for PS as a solid line and for P4VP as a dashed line.

3.3. Morphological characterization

Transmission electron micrographs were prepared in order to study the initial morphology and a possible change of morphology during shear and elongational flow with a constant deformation rate. Generally, the method of sample preparation plays an important role for the formation of microphase-separated structures. Structures with a more elaborated long-range order can be obtained by casting block copolymers from suitable solvents (preferentially non-selective solvents) such as chloroform, tetrahydrofuran or *N,N*-dimethylformamide. Van Ekenstein et al. state that the Flory-Huggins interaction parameter $\chi_{S,4VP}$ for PS-*b*-P4VP diblock copolymers ranges between 0.30 and 0.35.[47] In Table 3, the degree N of polymerization for the PS and

12

Polymer	M_n of PS (kg/mol)	M_n of P4VP (kg/mol)	N_S	N_{4VP}	χN
PS$_{89}$-b-P4VP$_{11}$[170]	157	13	1509	124	572
PS$_{74}$-b-P4VP$_{26}$[79]	64	15	618	140	265
PS$_{76}$-b-P4VP$_{24}$[159]	128	31	1231	294	534
PS$_{49}$-b-P4VP$_{51}$[60]	23	37	221	360	203
PS$_{48}$-b-P4VP$_{52}$[120]	60	60	521	629	403
PS$_{49}$-b-P4VP$_{51}$[131]	64	67	616	635	438

Table 3: Degree N of polymerization and product of the Flory-Huggins interaction parameter χ with N. The chosen value of the Flory-Huggins interaction parameter is $\chi = 0.35$.[47]

the P4VP blocks (denoted by N_S and N_{4VP}) and the product χN with the Flory-Huggins interaction parameter $\chi = \chi_{S,4VP}$ for the diblock copolymers are listed. The value of χN ranges between 203 and 572 and therefore is far above the limit of strong segregation.

The arrows in the transmission electron micrographs indicate the direction of shear or extension, respectively. Since iodine was used to obtain a contrast, the PS microphases appear bright and the P4VP microphases dark. Even though the P4VP microdomains contain the major fraction of iodine, a partial diffusion of iodine into the neighbored PS microphases might have been taken place. This effect possibly causes the diameter of the P4VP microphases to appear slightly larger than their true value. Regarding the results of the ^{1}H-NMR analysis as well as the high degree of polymerization, strong segregation of the microphases is expected for all three diblock copolymers with the highest molecular weight.

Figure 3(a) depicts transmission electron micrographs of the compression-molded PS$_{89}$-b-P4VP$_{11}$[170] diblock copolymer before shear (i), after shear (ii) and after elongation (iii). Neither shear nor elongational flow remarkably changed the microstructure of the polymer. Next to the typically ordered spherical morphology, a vast number of imperfections are perceptible which appear as poorly-ordered cylindrical microstructures.
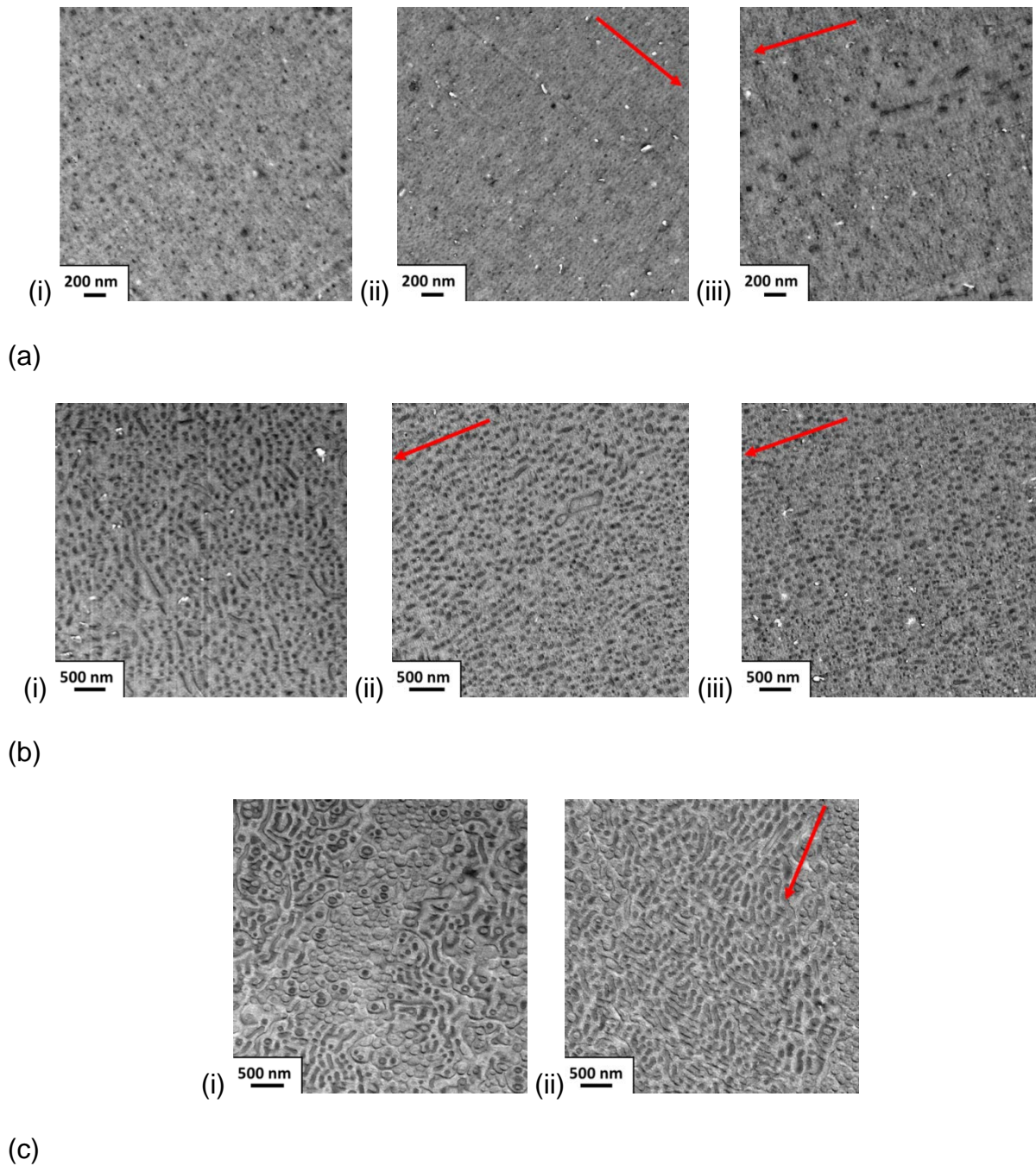
Figure 3: Transmission electron micrographs of (a) PS$_{89}$-*b*-P4VP$_{11}$[170], (b) PS$_{76}$-*b*-P4VP$_{24}$[159] and (c) PS$_{49}$-*b*-P4VP$_{51}$[131] diblock copolymers (i) before deformation, (ii) after a shear deformation with a shear rate of 0.1 s^{-1} for 10 s and (iii) after melt elongation with a Hencky strain rate of 0.1 s^{-1} for 10 s. The measurement temperature was 240 °C.

Transmission electron micrographs of the compression-molded PS$_{76}$-*b*-P4VP$_{24}$[159] diblock copolymer prior to shear (i), after shear (ii) and after elongation (iii) are presented in Figure 3(b). Neither shear nor elongational flow led to a significant change of microstructure even though a slight trend of shifting in the shear direction is recognizable. This result is possibly caused by the comparably long time during cooling

from 240 °C to a temperature below the glass transition temperature which was achieved through opening the heating chamber and the use of a piece of cotton wool (for quenching after elongation) which has been soaked in liquid nitrogen. The micrographs show a cylindrical microstructure with a similar size of the P4VP microdomains. However, the cylinders are not hexagonally packed in the observed areas. For the PS$_{49}$-*b*-P4VP$_{51}$[131] diblock copolymer, only shear experiments were accomplished. It was impossible to analyze a sample that had been extended under uniaxial loading due to brittle fracture. Nevertheless, the transmission electron micrographs before and after shear depict a rather complicated microstructure. Next to the presence of partially lamellar structures, large PS microspheres with a low P4VP content and micellar structures are recognizable. In order to interpret these variant microstructures, the results of GPC analysis and the sample preparation have to be taken into account. The GPC measurements revealed that the PS$_{49}$-*b*-P4VP$_{51}$[131] diblock copolymer exhibits a bimodal molecular weight distribution with a distinct peak at a molecular weight of approximately 70 kg/mol corresponding to PS homopolymer. A very rough estimate shows that 5 wt% of PS homopolymer is included in the PS-*b*-P4VP diblock copolymer with a rather broad molecular weight distribution due to varying P4VP chain lengths (caused by solubility problems of P4VP in THF) which led to partial termination of polymerization after the addition of the second monomer. Hereby, uncontrolled chain termination is accountable for the observed bimodal distribution which is responsible for the mixture of a cylindrical and a lamellar morphology. A partly comparable structure was found in the work of Krämer et al. on nanoporous silica structures from polybutadiene-*b*-poly(2-vinylpyridine) diblock copolymer templates.[48] The authors described the microstructure as a micellar structure close to the transition to a lamellar microstructure. Additionally, the sample preparation which was used in the work of Krämer et al. did not let the sample to attain an equilibrium state. The applied method of compression-molding for sample preparation cannot be compared to sample preparation from solvent casting. In the case of solvent cast films, the slow evaporation of a non-selective solvent for the polymer leads to a film close to an equilibrium state. Nevertheless, in this work the morphological and the rheological properties of the diblock copolymers are correlated and therefore the compression molding was chosen as preparation method. Furthermore, in case that a PS-*b*-P4VP diblock copolymer with a symmetrical composition underwent a large amplitude shear oscillation experiment, a broken lamellar structure occurred.[33] This broken lamellar structure is similar to the structure in Figure 3(c).
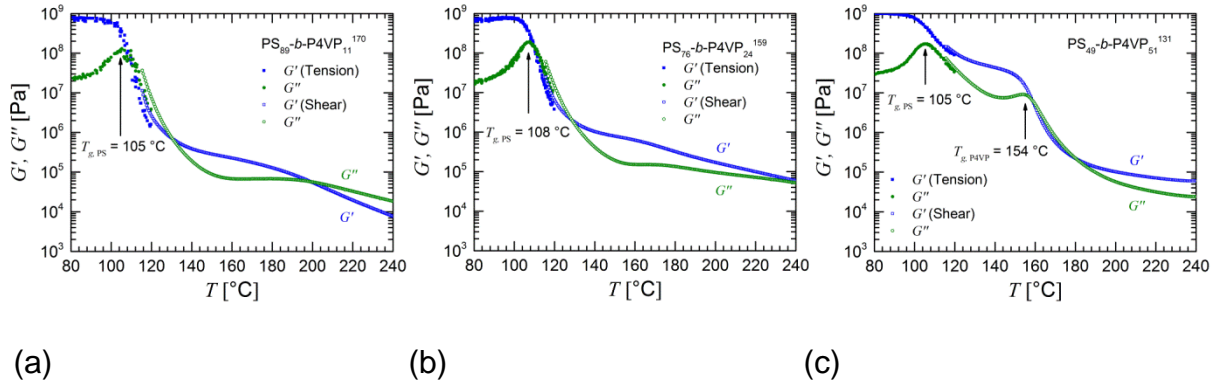
Figure 4: Storage modulus G' and loss modulus G'' as a function of temperature T obtained by dynamic-mechanical-thermal analysis (DMTA). The frequency was $f = 1\,\text{Hz}$.

3.4. Dynamic-mechanical-thermal analysis (DMTA)

A first impression of the influence of composition and morphology on the temperature-dependent dynamic moduli is given by the results of the dynamic-mechanical-thermal analysis, see Figure 4. The diblock copolymers PS$_{89}$-b-P4VP$_{11}$[170], PS$_{76}$-b-P4VP$_{24}$[159] and PS$_{49}$-b-P4VP$_{51}$[131] were selected for DMTA experiments because of their comparable molecular weight and significantly different PS/P4VP ratios. Generally, the storage modulus G' decreases with temperature, see Figure 4. At room temperature, below the glass transition temperature of the polystyrene block, the PS and the P4VP blocks both are in the glassy state. Here the storage modulus G' increases with the mass fraction of P4VP, i.e. at a temperature of 25 °C one has $G' = 0.86\,\text{GPa}$ for PS$_{89}$-b-P4VP$_{11}$[170], $G' = 0.92\,\text{GPa}$ for PS$_{76}$-b-P4VP$_{24}$[159] and $G' = 1.07\,\text{GPa}$ for PS$_{49}$-b-P4VP$_{51}$[131]. In the interval around 105 °C, the polystyrene block softens (glass transition of PS) which is associated with a local maximum of the loss modulus G''. At higher temperatures, the entanglement plateau of the polystyrene block appears. In the temperature interval between the glass transition temperatures of the PS and the P4VP blocks, the rubbery PS microphase is mechanically reinforced by the glassy P4VP blocks. In this regime, the storage modulus G' also increases with P4VP fraction. In the temperature interval around 150 °C, the glass transition of the P4VP block takes place. The values of the dynamic moduli result from a superposition of the continuous softening of the PS microphase and the glass transition of the P4VP block. Consequently, a maximum of the loss modulus can be only anticipated for the diblock copolymer with the highest mass fraction of P4VP, i.e. PS$_{49}$-b-P4VP$_{51}$[131]. At higher temperatures, the dynamic moduli moderately decrease. This decrease of dynamic moduli with temperature is mostly pronounced for the diblock copolymer PS$_{89}$-b-P4VP$_{11}$[170] with the largest PS fraction and the spherical morphology. The only slight decrease of the dynamic moduli for the other two diblock copolymers is caused by the

Polymer	G_N^0 (Pa)	τ_e (s)	T_∞ (°C)	c_1	c_2 (K)
PS	1.74×10^5	25.0	54.8	6.2 ± 0.1	105.2 ± 1.0
PS_{89}-b-$P4VP_{11}^{170}$	2.67×10^5	25.0	51.4	6.5 ± 0.1	108.6 ± 1.2
PS_{74}-b-$P4VP_{26}^{79}$	7.61×10^5	10.0	73.4	5.0 ± 0.8	86.6 ± 8.9
PS_{76}-b-$P4VP_{24}^{159}$	6.31×10^5	15.8	67.8	5.3 ± 0.3	92.2 ± 3.5
PS_{49}-b-$P4VP_{51}^{60}$	2.67×10^4	-	127.7	5.0 ± 0.0	32.3 ± 0.0
PS_{49}-b-$P4VP_{51}^{131}$	7.19×10^4	-	116.6	8.3 ± 0.4	43.4 ± 4.1
P4VP	2.75×10^5	-	53.8	13.4 ± 1.0	106.2 ± 12.0

Table 4: Plateau modulus G_N^0, equilibration time τ_e at $T = 120$ °C and WLF parameters c_1 and c_2 of PS-b-P4VP diblock copolymers of this study. The reference temperature T_{ref} for the WLF fit is 160 °C. The data for pristine polystyrene and poly(4-vinylpyridine) are taken from Schulze et al.[15]

microphase-separated structure with a much larger interfacial area than the spherical morphology, cf. the discussion of the master curves.

3.5. Frequency sweeps

Linear viscoelastic shear oscillations at a constant temperature allow for a quantitative evaluation of the dynamic moduli G' and G''. The results of our investigations are shown in Fig. 5 for a reference temperature of 160 °C. Figure 5(a) depicts the master curve for the diblock copolymer PS_{89}-b-$P4VP_{11}^{170}$ with a spherical morphology. At high frequencies (corresponding to low temperatures), the transition to the glass transition of the polystyrene block can be seen. A detailed inspection of the data of all diblock copolymers reveals that the crossover of the storage and the loss modulus in this regime is shifted to higher frequencies (i.e. corresponding to lower temperatures) for a lower molecular weight, see the values of the equilibration time τ_e in Table 4. The value of the equilibration time is given by $\tau_e = 2\pi/\omega_c$ where ω_c is the crossover frequency of G' and G'' in the high frequency limit. This result is in qualitative agreement with the Fox-Flory equation which describes the dependence of glass transition temperature on molecular weight. Our data indicate that the crossover frequency ω_c is influenced by the Rouse modes of the polystyrene block, and the molecular weight dependence of the free volume and monomeric friction coefficient can be clearly seen from the ω_c data. At intermediate frequencies, the entanglement plateau of the polystyrene block appears. The viscoelastic behavior at even lower frequencies is strongly influenced by the microphase-separated morphology. In case of the diblock copolymer with a spherical morphology, a shoulder of the storage modulus at low frequencies appears (Fig. 5(a)). This shoulder is an indication of increased elasticity which is caused by the

(a)   (b)   (c)
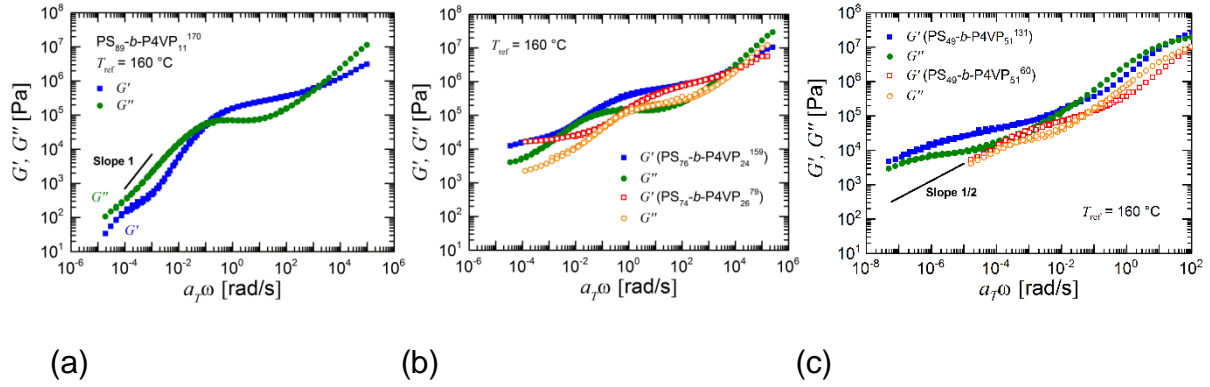
Figure 5: Master curves of the dynamic moduli G' and G'' as a function of angular frequency ω. The reference temperature is $T_{\text{ref}} = 160\,°\text{C}$. The diblock copolymers are: (a) PS$_{89}$-*b*-P4VP$_{11}$[170] (spherical morphology). (b) PS$_{74}$-*b*-P4VP$_{26}$[79] and PS$_{76}$-*b*-P4VP$_{24}$[159] (cylindrical morphology). (c) PS$_{49}$-*b*-P4VP$_{51}$[60] and PS$_{49}$-*b*-P4VP$_{51}$[131] (lamellar morphology).

interfacial tension between the PS and the P4VP microphases and the microphase-separated structure.

Figure 5(b) shows the influence of the molecular weight on the dynamic moduli G' and G'' for two diblock copolymers with a similar PS/P4VP ratio (approximately 75:25). A larger molecular weight leads to a larger entanglement plateau. In case of the diblock copolymer with a cylindrical morphology, a plateau of the storage modulus at low frequencies can be seen (Fig. 5(b)). The value of the storage modulus G' in the low frequency range is in the order of 10^4-10^5 Pa, in agreement with results of previous studies.[38] The value of G' in this plateau regime also marginally depends on molecular weight. The construction of a master curve for diblock copolymers with a lamellar morphology is shown in Fig. 5(c). For the diblock copolymer PS$_{49}$-*b*-P4VP$_{51}$[60] only the temperatures of 160, 180 and 200 °C were used for the construction of the master curve, since at higher temperatures morphological changes appeared. In case of the diblock copolymers with a lamellar morphology, the crossover to the $\omega^{1/2}$ regime can be anticipated (Fig. 5 (c)).[32] For both block copolymers with different molecular weights, only imperfect master curves have been achieved for these diblock copolymers with a symmetric composition. In the case of a symmetric composition, both blocks equally contribute to the dynamic response leading to a more complex or even an impossible shift behavior.

The plateau modulus G_N^0 was calculated based on the experimental data of 140 °C according to the method of Wu which defines the plateau modulus as the minimum of the loss tangent, i.e. $G_N^0 = G'(\omega)_{\tan\delta\rightarrow\text{minimum}}$.[49] The results of our analysis are listed in Table 4. The plateau modulus G_N^0 increases with P4VP fraction. This result shows that

the storage modulus in the entanglement regime is associated with a mechanical reinforcement effect caused by the P4VP microdomains.

In Figure 6 the shift factor a_T as a function of temperature T is plotted. The reference temperature is $T_{\text{ref}} = 160\,°\text{C}$. By fitting the Williams-Landel-Ferry (WLF) equation

$$\log a_T = -\frac{c_1(T-T_{\text{ref}})}{c_2+(T-T_{\text{ref}})} \tag{1}$$

the parameters c_1 and c_2 and the Vogel temperature $T_\infty = T_{\text{ref}} - c_2$ were determined (see Table 4). The diblock copolymers PS$_{89}$-*b*-P4VP$_{11}$[170], PS$_{76}$-*b*-P4VP$_{24}$[159] and PS$_{74}$-*b*-P4VP$_{26}$[79] show a similar behavior and WLF parameters due to the dominant influence of the PS matrix (cf. the curve for pristine PS). The c_1 values of these diblock copolymers are roughly similar. However, the value of c_2 decreases with the molecular weight of the polystyrene block. On the other hand, the diblock copolymers PS$_{49}$-*b*-P4VP$_{51}$[60] and PS$_{49}$-*b*-P4VP$_{51}$[131] are significantly influenced by the viscoelastic properties of the P4VP microphase and therefore the curves of the shift factor differ significantly in shape. Because of the larger P4VP fraction with a glass transition temperature in the order of 150 °C, the shift factor a_T decreases more strongly with temperature than for the diblock copolymers with the polystyrene matrix. Consequently, the WLF parameters show a pronounced composition effect. The relevance of the contribution of the block with a higher T_g was also observed for a lamellar polystyrene-polyisoprene diblock copolymer.[24] In the latter case, polyisoprene has a very low value of T_g and thus the shift behavior was dominated by the polystyrene block with a higher T_g than polyisoprene. In Fig. 6 the shift factor of the homopolymers PS and P4VP obtained by broadband dielectric spectroscopy (BDS) are presented which agree fairly well with the rheologically obtained shift factor. Consequently, the temperature dependence of the rheologically and dielectrically obtained relaxation times of the α-process (glass transition) are similar.
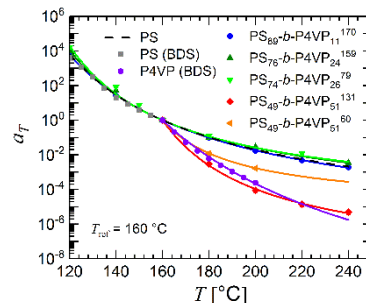
Figure 6: Shift factor a_T as a function of temperature T. The reference temperature is $T_{\text{ref}} = 160\,°\text{C}$. The data determined by broadband dielectric spectroscopy are denoted by "BDS."

3.6. Shear and elongational viscosity at constant deformation rate

Whereas the shear oscillations were performed at a low shear amplitude (linear viscoelastic regime), stress-growth experiments with a constant shear and extensional rate, respectively, allow one to probe the nonlinear behavior. The results of our measurements are depicted in Figures 7 and 8. In Figures 7(a) and (b), the transient shear viscosity $\eta(t)$ is plotted for diblock copolymers with a cylindrical and a lamellar morphology, respectively. In both cases, the molecular weight was also varied. An increase of molecular weight yields an increase of time-dependent viscosity. Furthermore, Figures 7(a) and (b) show that the shear viscosity at large times decreases with shear rate which is called structureviscous (pseudoplastic) behavior. In the subsequent relaxation interval (Figures 7(c) and (d)), the stress decays more rapidly with increasing shear rate in the preceding shear interval.
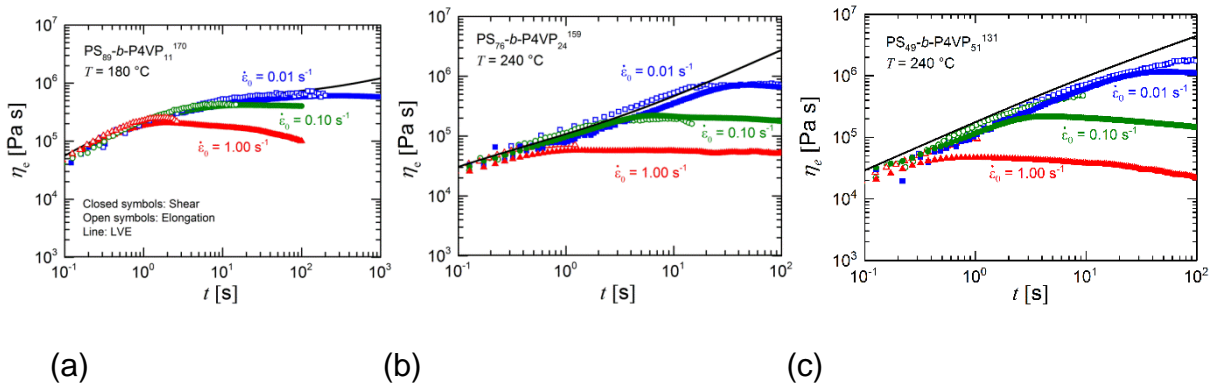
In Figure 8, the transient shear viscosity $\eta(t)$ is multiplied with the Trouton ratio of 3 in order to compare the shear viscosity data with the measured extensional viscosity $\eta_e(t)$. The linear viscoelastic prediction is also shown as solid line. The linear viscoelastic prediction was obtained by fitting a relaxation time spectrum $\{\tau_k, g_k\}_{1 \leq k \leq m}$ (relaxation time τ_k with modulus g_k) with m modes to the master curve for the dynamic moduli G' and G'' using the software NLREG[50, 51]. Then the extensional viscosity $\eta_e(t)$ in the linear regime is given by

$$\eta_e(t) = 3 \sum_{k=1}^{m} \tau_k g_k [1 - \exp(-t/\tau_k)] \tag{2}$$

Figure 8(a) shows the time-dependent extensional viscosity for the diblock copolymers. Our experimental data show that a reasonable agreement of the threefold of the shear viscosity and the measured extensional viscosity exists. This result indicates that similar deformation processes take place in shear and elongation, even in the regime of nonlinear deformations. In shear, the diblock copolymers are associated with a structureviscous behavior which is also commonly seen for homopolymers. For homopolymers, the structureviscous behavior is caused by disentanglement effects. The structureviscous behavior is only moderately pronounced for the diblock copolymer with a spherical morphology (PS_{89}-b-$P4VP_{11}^{170}$). The structureviscous effect can be much more seen for the diblock copolymers with a cylindrical and a lamellar morphology, see Figures 8(b) and (c). The peak appears at a similar strain value which can be explained with a rearrangement of morphology. Since the behavior in shear and elongation is similar, we assume that similar morphological rearrangements (i.e. a sliding of the microphase-separated domains) take place.
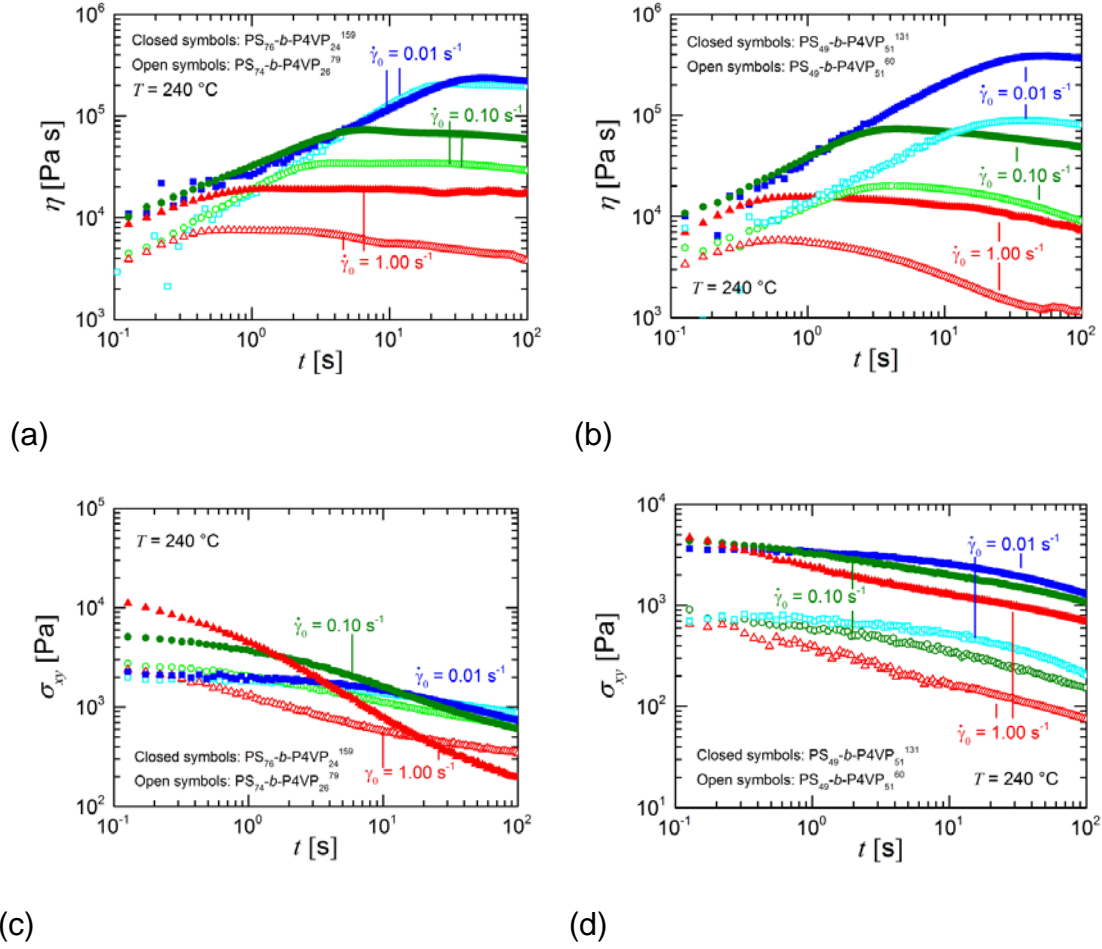
Figure 7: Comparison of the transient shear viscosity $\eta(t)$ of the diblock copolymers for (a) two diblock copolymers with a cylindrical morphology (PS$_{74}$-*b*-P4VP$_{26}$[79] and PS$_{76}$-*b*-P4VP$_{24}$[159]) and (b) two diblock copolymers with a lamellar morphology (PS$_{49}$-*b*-P4VP$_{51}$[60] and PS$_{49}$-*b*-P4VP$_{51}$[131]). In (c) and (d) the measured shear stress σ_{xy} in the subsequent relaxation interval is shown for these diblock copolymers. The measurement temperature was 240 °C. The shear rates are indicated.

Figure 8: Transient shear (multiplied with the Trouton ratio of 3, closed symbols) and extensional viscosity $\eta_\mathrm{e}(t)$ (open symbols) for the three diblock copolymers with the largest molecular weight. The solid line is the linear viscoelastic (LVE) prediction of the

extensional viscosity. The diblock copolymers are (a) PS_{89}-b-$P4VP_{11}$[170], (b) PS_{76}-b-$P4VP_{24}$[159] and (c) PS_{49}-b-$P4VP_{51}$[131].

A slightly less pronounced strain-softening of block copolymers has been also observed by Takahashi et al. for poly(styrene-*block*-ethylene-butylene-*block*-styrene) block copolymers.[37]

We also comment on the homogeneity of the sample during shear and elongation. Generally, homopolymers deform more uniformly than filled polymers and block copolymers. In oscillatory shear flow, edge fracture may occur at large deformations.[52] The deformation of the diblock copolymer PS_{49}-b-$P4VP_{51}$[60] at a shear strain of $\gamma = 3.0$ is shown in Figure 9(a). The applied shear rate was $\dot{\gamma}_0 = 0.10\ s^{-1}$ and hence the video image corresponds to a deformation time of 30 s. The figure clearly shows that the deformation of the sample was uniform. In melt elongation, a uniform deformation is also achieved up to a Hencky strain in the order of 1. Figures 9(b) and (c) present the diblock copolymer PS_{76}-b-$P4VP_{24}$[159] before deformation and after stretching up to a Hencky strain of 1 at a Hencky strain rate of 0.1 s⁻¹. A uniform deformation is observed. At much higher values of Hencky strain, necking and failure of the sample occur. Such analysis of failure modes has been recently performed for homopolymer melts.[53]

3.7. Broadband dielectric spectroscopy

In order to probe the relaxation behavior which is associated with the electric dipole moment, broadband dielectric spectroscopy was performed and the complex permittivity $\varepsilon^* = \varepsilon' - i\varepsilon''$ was determined. These measurements give additional information in temperature intervals where rheological data could not be achieved with the available experimental setup (e.g., below a measurement temperature of 140 °C for equal concentrations of P4VP and PS). Furthermore, the temperature dependence of the relaxation processes measured by rheological and dielectric techniques, respectively, was compared. The three diblock copolymers with different morphologies and the highest molecular weight (PS_{89}-b-$P4VP_{11}$[170], PS_{76}-b-$P4VP_{24}$[159] and PS_{49}-b-$P4VP_{51}$[131]) were chosen for these experiments. Figure 10 presents the dielectric loss ε'' as a function of temperature T in the range from -50 to 250 °C at a frequency of $f = 10000\ Hz$ for these diblock copolymers. The maxima of the dielectric loss ε'' can be related to specific relaxation processes. The homopolymers PS and P4VP were measured under the same conditions in the temperature range from -50 to 200 °C and are also displayed in Figure 10. The temperature-dependent dielectric loss ε'' depicts several relaxation peaks. A clearly pronounced maximum occurs at a temperature of approximately 0 °C for the samples with a non-zero fraction of P4VP. The intensity
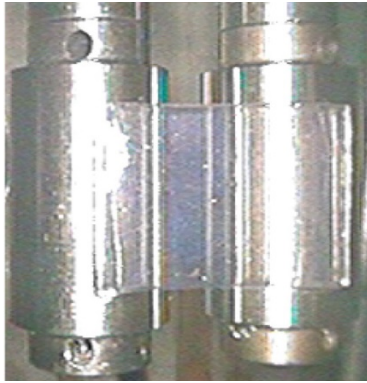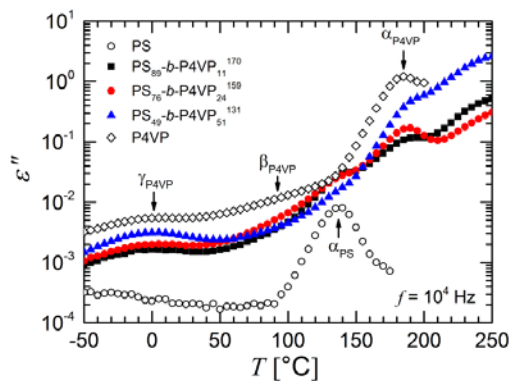
Figure 9: Deformation of diblock copolymers: (a) Diblock copolymer PS$_{49}$-*b*-P4VP$_{51}$[60] at a shear strain of $\gamma = 3.0$ at an applied shear rate of $\dot{\gamma}_0 = 0.10\,\text{s}^{-1}$. (b) Diblock copolymer PS$_{76}$-*b*-P4VP$_{24}$[159] before the melt elongational test. (c) Diblock copolymer PS$_{76}$-*b*-P4VP$_{24}$[159] at a Hencky strain of 1.0. The Hencky strain rate was 0.1 s^{-1}. The measurement temperature in (a) to (c) was 240 °C.

Figure 10: Results of dielectric measurements for PS$_{89}$-*b*-P4VP$_{11}$[170], PS$_{76}$-*b*-P4VP$_{24}$[159], PS$_{49}$-*b*-P4VP$_{51}$[131], pristine PS and P4VP. The dielectric loss ε'' at a frequency of $f = 10\,\text{kHz}$ is plotted as a function of temperature T.

of the peak rises with increasing P4VP fraction. Maiz et al. investigated a PS-*b*-P4VP diblock copolymer with a number average of the molecular weight of 69 kg/mol and a

23

PS/P4VP ratio of 74/26.[42] According to their work, this process at low temperatures can be identified with the γ-relaxation of P4VP. It can be related to the mobility of P4VP rings in poorly packed regions in P4VP homopolymers and at the interface between PS and P4VP in diblock copolymers.[42] Another distinct local maximum of the dielectric loss ε'' appears at a temperature of approximately 140 °C for the pristine PS homopolymer and the diblock copolymers. This relaxation process is associated with the α-relaxation of the PS microphase, since the glass transition temperature of high molecular weight polystyrene is about 105 °C (cf. the results of the DSC analysis). The intensity of the maximum increases with the PS fraction of the diblock copolymers. Additionally, Maiz et al. detected a maximum at slightly lower temperatures which is interpreted as the β-relaxation.[42] This process was not recognizable in the temperature dependent presentation, but is observed and discussed in the context of the frequency sweeps. Furthermore, a clearly visible maximum of the dielectric loss of pristine P4VP and the diblock copolymers occurs at a temperature of approximately 185 °C which can, in reasonable agreement with the results of the DSC analysis, be related to the α-relaxation of the P4VP phase. As for the previously discussed relaxation processes, the intensity of the maximum of the dielectric loss ε'' increases with P4VP fraction in the diblock copolymers. In case of the P4VP homopolymer and the PS$_{49}$-b-P4VP$_{51}$[131] diblock copolymer, the poor pronunciation of the peak can be explained with a significant contribution of the direct current conductivity at high temperatures due to a high P4VP content.

The results of isothermal measurements (frequency sweeps) are shown in Figure 11 which presents the dielectric loss ε'' as a function of frequency f for the three diblock copolymers. The γ-relaxation of the P4VP homopolymer and the three diblock copolymers can be clearly seen at a frequency of $f = 1000\,\text{Hz}$ at T = -25 °C (Figure (13(a)). The peak position does not depend on the diblock copolymer composition. However, the peak intensity increases with P4VP fraction. Furthermore, the γ-relaxation is comparably weak and can only be detected at low temperatures, since it is associated with local rearrangements, i.e. the dynamics of 4VP rings in poorly packed regions. The β-relaxation process can be associated to the mobility of the polymer backbones of P4VP chains below the glass transition temperature. As displayed in Figure 11(b), it slightly differs in peak position and intensity. This behavior can be attributed to the fact that the β-relaxation process is partially superimposed by the α-relaxation process of the PS block. The influence of the PS fraction is discussed in more detail with the analysis of the activation energy E_A and the relaxation time τ_∞ at an infinite temperature. At a temperature of 130 °C (see Figure 11(c)), the α-relaxation of PS can be detected for pristine PS, PS$_{89}$-b-P4VP$_{11}$[170] and PS$_{76}$-b-P4VP$_{24}$[159] at a frequency of approximately $f = 1000\,\text{Hz}$. The maximum of the

24

dielectric loss ε'' of PS$_{49}$-b-P4VP$_{51}$[131] cannot be observed at a first glance because of the only comparably low weight fraction of PS. However, a closer examination (fit procedure) of this curve indicates the existence of the α-relaxation at a similar position. The linear increase of ε'' at low frequencies can be explained with

(a)

(b)

(c)

(d)
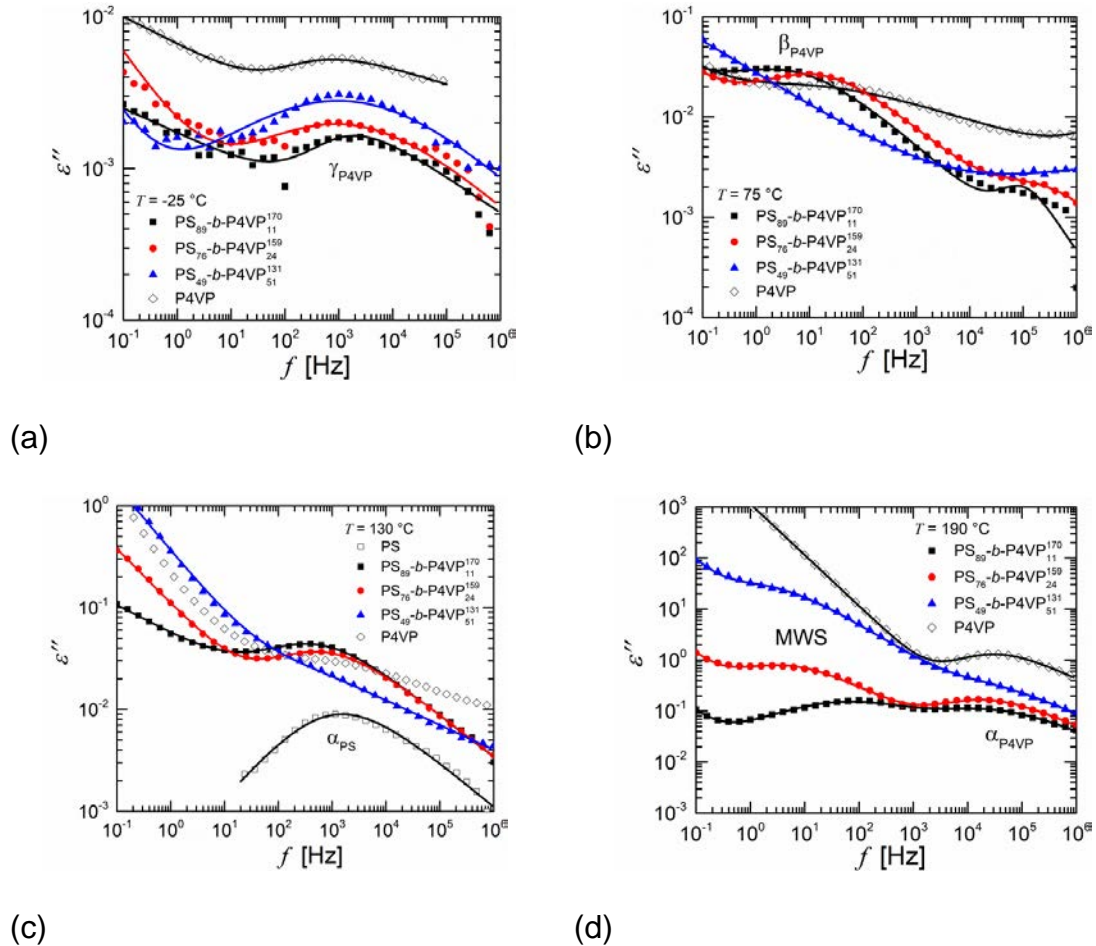
Figure 11: Dielectric loss ε'' as a function of frequency f at temperatures T of (a) -25 °C, (b) 75 °C, (c) 130 °C and (d) 190 °C for the three diblock copolymers PS$_{89}$-b-P4VP$_{11}$[170], PS$_{76}$-b-P4VP$_{24}$[159] and PS$_{49}$-b-P4VP$_{51}$[131] as well as the homopolymers PS and P4VP. The results of the HN fits Eq. (5) are shown as solid lines.

the contribution of direct current in the PS melt and the upcoming relaxation process of the P4VP phase. In comparison with the P4VP homopolymer at 190 °C, the α-relaxation of P4VP can be also detected at $f = 10^5$ Hz for the diblock copolymers. The intensity of the maximum qualitatively also increases with the P4VP fraction.

Table 5: Results of the fit of the imaginary part ε'' of the Havriliak-Negami function Eq. (5) to the dielectric loss ε'' at isothermal measurements in Figure 13 at a temperature of (a) -25 °C, (b) 75 °C, (c) 130 °C and (d) 190 °C ($\tau_k = \tau_{\text{HN},k}$). In (c) and (d) the parameters of the homopolymers are associated with the corresponding mode of the diblock copolymers.

(a)

Polymer	$\Delta\varepsilon_1$ (10^{-2})	τ_1 (10^4 s)	α_1	β_1	$\Delta\varepsilon_2$ (10^{-3})	τ_2 (10^{-4} s)	α_2	β_2
PS$_{89}$-b-P4VP$_{11}$^{170}	2.48	0.05	1.00	0.17	5.64	1.95	0.75	0.36
PS$_{76}$-b-P4VP$_{24}$^{159}	253	10	0.59	0.88	13.20	2.29	0.38	0.84
PS$_{49}$-b-P4VP$_{51}$^{131}	244	10	0.64	0.98	20.70	1.60	0.34	1.00
P4VP	21.60	1.61	0.34	0.59	36.50	9.40	0.70	0.13

(b)

Polymer	$\Delta\varepsilon_1$ (10^1)	τ_1 (10^4 s)	α_1	β_1	$\Delta\varepsilon_2$ (10^{-1})	τ_2 (10^{-2} s)	α_2	β_2	$\Delta\varepsilon_3$ (10^{-2})	τ_3 (10^{-7} s)	α_3	β_3
PS$_{89}$-b-P4VP$_{11}$^{170}	0.10	6.43	1.00	1.00	1.61	36.50	0.56	0.71	0.37	9.05	0.64	1.00
PS$_{76}$-b-P4VP$_{24}$^{159}	3.43	10.00	80	0.83	1.14	4.92	0.63	0.64	0.45	7.28	0.67	1.00
PS$_{49}$-b-P4VP$_{51}$^{131}	4.23	10.00	0.71	0.90	1.01	39.30	0.39	1.00	2.98	0.99	0.25	1.00
P4VP	1.01	4.98	0.76	0.73	1.30	1.07	0.0.37	0.93	3.22	1.84	0.42	0.72

(c)

Polymer	$\Delta\varepsilon_1$	τ_1 $(10^3\,\text{s})$	α_1	β_1	$\Delta\varepsilon_2$ (10^{-1})	τ_2 $(10^{-4}\,\text{s})$	α_2	β_2
PS	-	-	-	-	0.39	1.69	0.61	0.72
PS_{89}-b-$P4VP_{11}^{170}$	6.63	100	0.30	1.00	1.48	5.00	0.61	0.74
PS_{76}-b-$P4VP_{24}^{159}$	3.09	0.04	1.00	0.54	1.50	4.22	0.61	0.69
PS_{49}-b-$P4VP_{51}^{131}$	297	5.02	0.79	0.80	1.11	25.40	0.53	0.46

(d)

Polymer	σ_0 $(10^{-14}\,\text{S/cm})$	$\Delta\varepsilon_1$	τ_1 $(10^{-2}\,\text{s})$	α_1	β_1	$\Delta\varepsilon_2$ (10^{-1})	τ_2 $(10^{-5}\,\text{s})$	α_2	β_2
PS_{89}-b-$P4VP_{11}^{170}$	0.48	0.72	0.28	0.49	1.00	3.71	0.87	0.60	0.74
PS_{76}-b-$P4VP_{24}^{159}$	6.68	2.96	4.21	0.60	1.00	6.04	0.98	0.64	0.79
PS_{49}-b-$P4VP_{51}^{131}$	468	89.30	10.40	0.64	1.00	8.06	1.34	0.72	0.57
P4VP	63700	-	-	-	-	45.20	0.73	0.73	0.71

27

(a)
(b)
(c)
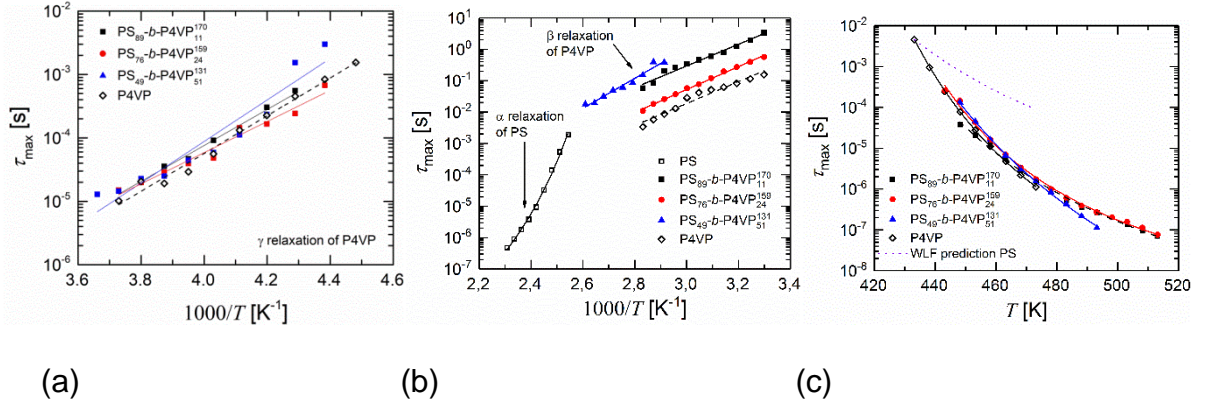
Figure 12: Relaxation time τ_{max} as a function of the inverse of absolute temperature T of the (a) γ-relaxation of P4VP, (b) β-relaxation of P4VP and α-relaxation process of PS and (c) α-relaxation process of P4VP for the homopolymers and the PS$_{89}$-b-P4VP$_{11}$[170], PS$_{76}$-b-P4VP$_{24}$[159] and PS$_{49}$-b-P4VP$_{51}$[131] diblock copolymers of this study. The fits of Eqs. (6) and (7) are indicated as lines.

Furthermore, the data of pristine P4VP show a high conductivity at low frequencies, whereas the diblock copolymer curves at low frequencies reveal a second local maximum of ε''. This maximum can be related to Maxwell-Wagner-Sillars polarization (MWS) at inner dielectric boundary layers which appear at the interface between the PS and the P4VP microphases. The MWS polarization can be quantitatively discussed using the MWS theory.[54] In the frequency interval of MWS relaxation, one can approximate the dielectric response of the block copolymers by assuming a direct current (d.c.) conductivity σ and a real, frequency-independent dielectric permittivity ε for each microphase. Then the theory of heterogeneous media can be applied.[54] Assuming this approximation, one finds a single-mode Debye relaxation process, where the relaxation time τ_{MWS} is given by

$$\tau_{\mathrm{MWS}} = \varepsilon_0 \left[\varepsilon_{\mathrm{PS}} - n(\varepsilon_{\mathrm{PS}} - \varepsilon_{\mathrm{P4VP}})(1 - \Phi_{\mathrm{P4VP}})\right]/\left[\sigma_{\mathrm{PS}} - n(\sigma_{\mathrm{PS}} - \sigma_{\mathrm{P4VP}})(1 - \Phi_{\mathrm{P4VP}})\right] \quad (3)$$

with the shape factor n and the permittivity ε_0 of the vacuum. The symbols ε and σ denote the real dielectric permittivity and the direct current conductivity of PS and P4VP, respectively. Taking the values $\varepsilon_{\mathrm{PS}} = 2.6$, $\varepsilon_{\mathrm{P4VP}} = 3.2$, $\sigma_{\mathrm{PS}} = 3.0 \times 10^{-11} \mathrm{S/m}$ and $\sigma_{\mathrm{P4VP}} = 6.4 \times 10^{-8} \mathrm{S/m}$ and fitting a single mode Havriliak-Negami function with a d.c. term for determining τ_{MWS} to the data of 190 °C one finds for the shape factor

$$n = \frac{\tau_{\mathrm{MWS}}\sigma_{\mathrm{PS}}/\varepsilon_0 - \varepsilon_{\mathrm{PS}}}{(1 - \Phi_{\mathrm{P4VP}})[\tau_{\mathrm{MWS}}(\sigma_{\mathrm{PS}} - \sigma_{\mathrm{P4VP}})/\varepsilon_0 - (\varepsilon_{\mathrm{PS}} - \varepsilon_{\mathrm{P4VP}})]} \quad (4)$$

$n = 0.233$ for $\Phi_{\mathrm{PS}} = 1 - \Phi_{\mathrm{P4VP}} = 0.89$, $n = 0.005$ for $\Phi_{\mathrm{PS}} = 0.76$ and $n = 0.000$ for $\Phi_{\mathrm{PS}} = 0.49$. Consequently, the shape factor determined by Eq. (4) decreases in the

order spheres – cylinders – lamellae for these block copolymers that were prepared by film casting.

The fraction of PS and P4VP distinctly influences the dielectric loss of the diblock copolymers in the range of the γ- and α-relaxation. The influence of the diblock copolymer composition on the β-relaxation is attributed to the overlap with the α-relaxation process of polystyrene. In order to analyze the temperature dependence of the identified characteristic relaxation times, the experimental data were fitted to the imaginary part of the Havriliak-Negami (HN) function

$$\varepsilon_{\mathrm{HN}}^{*}(\omega) = \varepsilon_{\infty} + \sum_{k=1}^{m} \frac{\Delta\varepsilon_k}{\left[1+(i\omega\tau_{\mathrm{HN},k})^{\alpha_k}\right]^{\beta_k}} \tag{5}$$

with m modes and the parameters $0 < \alpha_k, \beta_k \leq 1$. In Eq. (5) $\Delta\varepsilon_k$ is the dielectric strength of the kth mode, ε_{∞} the permittivity in the high frequency limit and $\tau_{\mathrm{HN},k}$ the characteristic relaxation time of the corresponding process. The parameter α_k describes the asymmetry and the parameter β_k the broadening of the dielectric loss ε'' as a function of angular frequency $\omega = 2\pi f$. The results of the fit procedure for the three chosen temperatures are shown in Figure 11 and listed in Table 5. In order to fit the experimental data, a direct current contribution $\varepsilon'' = i\sigma_0/(\varepsilon_0\omega)$ with up to three ($m \leq 3$) HN functions were used for the fit procedure. Here the direct current conductivity is denoted by σ_0. Each relaxation process that is described by the Havriliak-Negami function is associated with a maximum of the dielectric loss which is located at a certain frequency f_{max}. This frequency f_{max} at peak position is also evaluated by the fit software. In Figure 12, the temperature dependence of the relaxation times $\tau_{\mathrm{max}} = 1/(2\pi f_{\mathrm{max}})$ is presented. It has to be noted that specific relaxation processes partially superimpose. According to the results of the temperature sweeps, only the γ-relaxation of P4VP can be regarded as independent from other relaxation processes. Furthermore, the α-relaxation of the PS block of the diblock copolymers could not be determined quantitatively since it is located in the frequency interval between the β- and the α-relaxations of the P4VP phase. By fitting the Arrhenius equation with the universal gas constant R

$$\tau_{\mathrm{max}}(T) = \tau_{\infty} \exp[E_A/(RT)] \tag{6}$$

the activation energy E_A of the γ and the β processes and by fitting the Vogel-Fulcher-Tammann equation with temperature parameter T_A and Vogel temperature T_{∞}

$$\tau_{\mathrm{max}}(T) = \tau_{\infty} \exp[T_A/(T - T_{\infty})] \tag{7}$$

29

for the α process to the experimentally determined relaxation times τ_{max}, the relaxation time τ_∞ at an infinite temperature was determined, see Figure 12 and Table 6. In general, the uncertainty of this method is approximately 10%.[55]

Polymer	E_A^γ (kJ/mol)	τ_∞^γ (s)	E_A^β (kJ/mol)	τ_∞^β (s)	T_∞ (K)	τ_∞^α (s)
PS	-	-	-	-	328	4×10^{-13}
PS_{89}-b-$P4VP_{11}$[170]	54	4×10^{-16}	66	1×10^{-11}	352	5×10^{-12}
PS_{76}-b-$P4VP_{24}$[159]	47	9×10^{-15}	70	6×10^{-13}	383	5×10^{-11}
PS_{49}-b-$P4VP_{51}$[131]	63	7×10^{-18}	91	5×10^{-15}	337	4×10^{-15}
P4VP	57	7×10^{-17}	67	6×10^{-13}	366	1×10^{-12}

Table 6: Activation energy E_A, Vogel temperature T_∞ and relaxation time τ_∞ at an infinite temperature for the different relaxation processes determined by an Arrhenius fit Eq. (6) to the data of the $\beta-$ and $\gamma-$ relaxation and by a Vogel-Fulcher-Tammann fit Eq. (7) to the data of the $\alpha-$relaxation process.

In contrast to Maiz et al.[42] the activation energy E_A^γ and the relaxation time τ_∞^γ of the γ-process of the diblock copolymers do not remarkably differ from the one in the pristine P4VP homopolymer displayed in Figure 12(a). Whereas Maiz et al. found τ_∞^γ values of 10^{-17} s for the P4VP homopolymer and τ_∞^γ values of 10^{-12} s for the diblock copolymer, in this work τ_∞^γ ranged between 10^{-18} s for PS_{49}-b-$P4VP_{51}$[131] and 10^{-14} s for PS_{76}-b-$P4VP_{24}$[159]. This small difference can be explained by varying sample preparation techniques, since Maiz et al.[42] cast the film from chloroform whereas the samples in this work were produced by compression-molding.

The activation energy E_A^β and the relaxation time τ_∞^β of the β-relaxation process do not show a monotonic trend with P4VP fraction (Table 6). Since the β-relaxation process of the P4VP phase and the α-relaxation process of the PS phase are located in proximity to each other, these two processes mutually influence the position of the related peaks. On the contrary, the α-relaxation process of the P4VP microphase of the diblock copolymers is less influenced by other processes (Figure 12(c)). The values of the Vogel temperature T_∞ for PS_{76}-b-$P4VP_{24}$[159], PS_{49}-b-$P4VP_{51}$[131] and pristine P4VP range between 337 and 383 K and consequently are slightly larger than the value of 327 K of the rheological experiments. The relaxation time τ_∞^α of the homopolymer P4VP and of the diblock copolymers are in a similar time range. Only PS_{49}-b-$P4VP_{51}$[131] stands out with a significantly lower relaxation time. The difference can be explained

with a pronounced contribution of direct current conductivity of the P4VP microdomains leading to a larger statistical error of the fit procedure. The dotted line in Fig. 12(c) shows the WLF shift of the data in Fig. 6 using the rheologically obtained shift factor of the α process polystyrene. The β and γ processes are local processes which are not presented by our rheological data. Whereas the rheological shift behavior of the diblock copolymers is dominated by the PS matrix (cf. Fig. 6), the shift behavior determined by broadband dielectric spectroscopy (BDS) is dominated by the γ-process of P4VP.

4. Conclusions

This study elucidates the effect of composition (weight ratios of 89/11, 76/24 and 49/51) and morphology (spherical, cylindrical and lamellar) on the viscoelastic and dielectric properties of PS-*b*-P4VP diblock copolymers in the strongly segregated regime. The diblock copolymers were prepared by anionic polymerization in order to achieve a narrow polydispersity. In particular, the diblock copolymers are characterized by strain-softening in shear and extensional flows which was shown for these three different types of morphology (spherical, cylindrical and lamellar) in this work. Consequently, both in shear and elongation similar deformation processes take place. The viscoelastic properties of polystyrene-*block*-poly(4-vinylpyridine) diblock copolymers at small and large deformations are strongly influenced by the composition and the diblock copolymer morphology. The linear regime is determined by superposition and interfacial effects. Whereas the spherical and cylindrical morphologies are mostly determined by the PS microphase, the lamellar morphology is also strongly influenced by the P4VP block. At high frequencies (i.e. at large values of moduli and applied stress), the dynamic moduli result from a superposition of the properties of the two blocks. At low frequencies, effects of the microstructure play a dominant role (interfacial effects which are associated with microphase separation). Microstructural effects are less pronounced in the case of a large fraction of the majority phase (spherical morphology). A pronounced strain-softening behavior in shear and elongation (nonlinear deformations) in the melt state appears for the diblock copolymers with a cylindrical and a lamellar morphology. For a high weight fraction of the majority phase and a spherical morphology, respectively, strain-softening also takes place, but to a much lesser extent. Consequently, the degree of strain-softening of diblock copolymer melts can be tailored by the weight/volume ratio of the two blocks. The dielectric measurements reveal the superposition of different relaxation processes of the homopolymers and in addition a MWS polarization in case of the diblock copolymers. The appearance and the position of the glass transition of the two blocks in rheological (dynamic-mechanical-thermal analysis, master curve of dynamic moduli) and dielectric measurements results from a superposition of the relaxation processes of the two blocks.

31

Acknowledgement

References

[1] F.S. Bates, M.A. Hillmyer, T.P. Lodge, C.M. Bates, K.T. Delaney, G.H. Fredrickson, Mulitblock Polymers: Panacea or Pandora's Box, Science 336 (2012) 434-440.

[2] V. Abetz, P.F.W. Simon, Phase Behaviour and Morphologies of Block Copolymers, Advances in Polymer Science, Springer, Berlin, 2005, pp. 125-212.

[3] I. Erukhimovich, V. Abetz, R. Stadler, Microphase Separation in Ternary ABC Block Copolymers: Ordering Control in Molten Diblock AB Copolymers by Attaching a Short Strongly Interacting C Block, Macromolecules 30 (1997) 7435-7443.

[4] C.-C. Chao, T.-C. Wang, R.-M. Ho, P. Georgopanos, A. Avgeropoulos, E.L. Thomas, Robust Block Copolymer Mask for Nanopattering Polymer Films, ACS Nano 4(4) (2010) 2088-2094.

[5] V. Abetz, Isoporous Block Copolymer Membranes, Macromolecular Rapid Communications 36 (2015) 10-22.

[6] K. Sankhala, J. Koll, M. Radjabian, U.A. Handge, V. Abetz, A Pathway to Fabricate Hollow Fiber Membranes with Isoporous Inner Surface, Advanced Materials Interfaces 4(7) (2017) 1600991.

[7] R.G. Larson, The Structure and Rheology of Complex Fluids, Oxford University Press, New York, 1999.

[8] D.M. Hoyle, Q. Huang, D. Auhl, D. Hassell, H.K. Rasmussen, A.L. Skov, O.G. Harlen, Transient Overshoot Extensional Rheology of Long-Chain Branched Polyethylenes: Experimental and Numerical Comparisons Between Filament Stretching and Cross-Slot Flow, Journal of Rheology 57(1) (2013) 293-313.

[9] Q. Huang, M. Mangnus, N.J. Alvarez, R. Koopmans, O. Hassager, A New Look at Extensional Rheology of Low-Density Polyethylene, Rheologica Acta 55 (2016) 343-350.

[10] S.L. Wingstrand, M. van Drongelen, K. Mortensen, R.S. Graham, Q. Huang, O. Hassager, Influence of Extensional Stress Overshoot on Crystallization of LDPE, Macromolecules 50 (2017) 1134-1140.

[11] T.I. Burghelea, Z. Starý, H. Münstedt, On the "Viscosity Overshoot" during the Uniaxial Extension of a Low Density Polyethylene, Journal of Non-Newtonian Fluid Mechanics 166(19-20) (2011) 1198-1209.

[12] H. Münstedt, Rheological Properties and Molecular Structure of Polymer Melts, Soft Matter 7(6) (2011) 2273-2283.

[13] F.J. Stadler, C. Piel, K. Klimke, J. Kaschta, M. Parkinson, M. Wilhelm, W. Kaminsky, H. Münstedt, Influence of Type and Content of Various Comonomers on Long-Chain Branching of Ethene/α-Olefin Copolymers, Macromolecules 39 (2006) 1474-1482.

[14] M. Schulze, U.A. Handge, S. Rangou, J. Lillepärg, V. Abetz, Thermal Properties, Rheology and Foams of Polystyrene-*block*-Poly(4-vinylpyridine) Diblock Copolymers, Polymer 70 (2015) 88-99.

[15] M. Schulze, U.A. Handge, V. Abetz, Preparation and Characterisation of Open-Celled Foams Using Polystyrene-*b*-Poly(4-vinylpyridine) and Poly(4-methylstyrene)-*b*-Poly(4-vinylpyridine) Diblock Copolymers, Polymer 108 (2017) 400-412.

[16] F.S. Bates, G.H. Fredrickson, Block Copolymer Thermodynamics: Theory and Experiment, Annual Review of Physical Chemistry 41 (1990) 525-557.

[17] M.W. Matsen, F.S. Bates, Unifying Weak- and Strong-Segregation Block Copolymer Theories, Macromolecules 29(4) (1996) 1091-1098.

[18] J.M. Sebastian, C. Lai, W.W. Graessley, R.A. Register, Steady-Shear Rheology of Block Copolymer Melts and Concentrated Solutions: Disordering Stress in Body-Centered-Cubic Systems, Macromolecules 35 (2002) 2707-2713.

[19] J.M. Sebastian, C. Lai, W.W. Graessley, R.A. Register, G.R. Marchand, Steady-Shear Rheology of Block Copolymer Melts: Zero-Shear Viscosity and Shear Disordering in Body-Centered-Cubic Systems, Macromolecules 35 (2002) 2700-2706.

[20] T. Pakula, K. Saijo, H. Kawai, T. Hashimoto, Deformation Behavior of Styrene-Butadiene-Styrene Triblock Copolymer with Cylindrical Morphology, Macromolecules (1985) 1294-1302.

[21] M.B. Kossuth, D.C. Morse, F.S. Bates, Viscoelastic Behavior of Cubic Phases in Block Copolymer Melts, Journal of Rheology 43(1) (1999) 167-196.

[22] J. Zhao, B. Majumdar, M.F. Schulz, F.S. Bates, K. Almdal, K. Mortensen, D.A. Hajduk, S.M. Gruner, Phase Behavior of Pure Diblocks and Binary Diblock Blends of Poly(ethylene)-Poly(ethylethylene), Macromolecules 29 (1996) 1204-1215.

[23] P. Georgopanos, S. Rangou, T.G. Haenelt, C. Abetz, A. Meyer, V. Filiz, U.A. Handge, V. Abetz, Analysis of Glass Transition and Relaxation Processes of Low Molecular Weight Polystyrene-*b*-Polyisoprene Diblock Copolymers, Colloid and Polymer Science 292 (2014) 1877-1891.

[24] T.G. Haenelt, P. Georgopanos, C. Abetz, S. Rangou, D. Alisch, A. Meyer, U.A. Handge, V. Abetz, Morphology and Elasticity of Polystyrene-*block*-Polyisoprene Diblock Copolymers in the Melt, Korea-Australia Rheology Journal 26(3) (2014) 263-275.

[25] P. Georgopanos, U.A. Handge, C. Abetz, V. Abetz, Influence of Block Sequence and Molecular Weight on Morphological, Rheological and Dielectric Properties of Weakly and Strongly Segregated Styrene-Isoprene Triblock Copolymers, Polymer 104 (2016) 279-295.

[26] B.M. Yavitt, Y. Gai, D.-P. Song, H.H. Winter, J.J. Watkins, High Molecular Mobility and Viscoelasticity of Microphase-Separated Bottlebrush Diblock Copolymer Melts, Macromolecules 50 (2017) 396-405.

[27] Y. Takahashi, L. Fang, A. Takano, N. Torikai, Y. Matsushita, Viscoelastic Properties of Low Molecular Weight Symmetric Poly(styrene-*b*-2-vinylpyridine)s in the Ordered and Disordered States under Steady Shear Flow, Nihon Reoroji Gakkaishi 41(2) (2013) 83-91.

[28] L. Fang, Y. Takahashi, A. Takano, Y. Matsushita, A Separation Method of Responses from Large Scale Motions and Chain Relaxations for Viscoelastic Properties of Symmetric Poly(styrene-*b*-2-vinylpyridine)s in the Ordered State, Nihon Reoroji Gakkaishi 41(2) (2013) 93-99.

[29] A. Serghei, Polymer Nanofluidics by Broadband Dielectric Spectroscopy, in: F. Kremer (Ed.), Dynamics in Geometrical Confinement, Springer International Publishing Switzerland, Cham, 2014, pp. 165-177.

[30] M.F. Schulz, A.K. Khandpur, F.S. Bates, K. Almdal, K. Mortensen, D.A. Hajduk, S.M. Gruner, Phase Behavior of Polystyrene-Poly(2-vinylpyridine) Diblock Copolymers, Macromolecules 29 (1996) 2857-2867.

[31] L. Fang, Y. Takahashi, A. Takano, Y. Matsushita, Molecular Weight Dependence of Viscoelastic Properties for Symmetric Poly(styrene-*b*-2-vinylpyridine)s in the Nanophase Segregated Molten States, Macromolecules 46 (2013) 7097-7105.

[32] K. Kawasaki, A. Onuki, Dynamics and Rheology of Diblock Copolymers Quenched into Microphase-Separated States, Physical Review A 42 (1990) 3664-3666.

[33] F. Wode, L. Tzounis, M. Kirsten, M. Constantinou, P. Georgopanos, S. Rangou, N.E. Zafeiropoulos, A. Avgeropoulos, M. Stamm, Selective Localization of Multi-wall Carbon Nanotubes in Homopolymer Blends and a Diblock Copolymer. Rheological Orientation Studies of the Final Nanocomposites, Polymer 53 (2012) 4438-4447.

[34] A.P. Holt, J.R. Sangoro, Y. Wang, A.L. Agapov, A.P. Sokolov, Chain and Segmental Dynamics of Poly(2-vinylpyridine) Nanocomposites, Macromolecules 46 (2013) 4168-4173.

[35] U.A. Handge, M.F.H. Wolff, V. Abetz, S. Heinrich, Viscoelastic and Dielectric Properties of Composites of Poly(vinyl butyral) and Alumina Particles with a High Filling Degree, Polymer 82 (2016) 337-348.

[36] Y. Takahashi, N. Ochiai, Y. Matsushita, I. Noda, Viscoelastic Properties of Poly(2-vinylpyridine) in Bulk and Solution, Polymer Journal 28(12) (1996) 1065-1070.

[37] T. Takahashi, J.-I. Takimoto, K. Koyama, Elongational Viscosities of Random and Block Copolymer Melts, Journal of Applied Polymer Science 69 (1998) 1765-1774.

[38] E.M. McCready, W.R. Burghardt, Structural Response of a Prealigned Cylindrical Block Copolymer Melt to Extensional Flow, Journal of Rheology 59(4) (2015) 935-956.

[39] R. Mao, E.M. McCready, W.R. Burghardt, Structural Response of an Ordered Block Copolymer Melt to Uniaxial Extensional Flow, Soft Matter 10 (2014) 6198-6205.

[40] E.M. McCready, W.R. Burghardt, In Situ SAXS Studies of Structural Relaxation of an Ordered Block Copolymer Melt Following Cessation of Uniaxial Elongational Flow, Macromolecules 48 (2015) 264-271.

[41] A. Schönhals, F. Kremer, Broadband Dielectric Spectroscopy, Springer (Berlin) 2003.

[42] J. Maiz, W. Zhao, Y. Gu, J. Lawrence, A. Arbe, A. Alegría, T. Emrick, J. Colmenero, T.P. Russell, C. Mijangos, Dynamic Study of Polystyrene-*block*-Poly(4-vinylpyridene) Copolymer in Bulk and Confined in Cylindrical Nanopores, Polymer 55 (2014) 4057-4066.

[43] N. Sanno, I. Murakami, H. Yamamura, Dielectric β-Relaxation in Poly(2-vinylpyridine), Polymer Journal 8(3) (1976) 231-238.

[44] S. Madkour, H. Yin, M. Füllbrandt, A. Schönhals, Calorimetric Evidence for a Mobile Surface Layer in Ultrathin Polymeric Films: Poly(2-vinylpyridine), Soft Matter 11 (2015) 7942-7952.

[45] J. Aho, V.H. Rolón-Garrido, S. Syrjälä, M. Wagner, Measurement Technique and Data Analysis of Extensional Viscosity for Polymer Melts by Sentmanat Extensional Rheometer (SER), Rheologica Acta 49 (2010) 359-370.

[46] F.S. Bates, G.H. Fredrickson, Block Copolymers - Designer Soft Materials, Physics Today 52 (1999) 32.

[47] G.O.R.A. van Ekenstein, R. Meyboom, G. ten Brinke, O. Ikkala, Determination of the Flory-Huggins Interaction Parameter of Styrene and 4-Vinylpyridine Using Copolymer Blends of Poly(styrene-*co*-4-vinylpyridine) and Polystyrene, Macromolecules 33(10) (2000) 3752-3756.

[48] E. Krämer, S. Förster, C. Göltner, M. Antonietti, Synthesis of Nanoporous Silica with New Pore Morphologies by Templating the Assemblies of Ionic Block Copolymers, Langmuir 14 (1998) 2027-2031.

[49] S. Wu, Chain Structure and Entanglement, Journal of Polymer Science Part B: Polymer Physics 27(19) (1989) 723-741.

[50] Freiburg Materials Research Center, Service Group Scientific Data Processing, NLREG, (Software Version May 2008).

[51] J. Honerkamp, J. Weese, A Note on Estimating Master Curves, Rheologica Acta 32 (1993) 57-64.

[52] K.M. Mattes, R. Vogt, C. Friedrich, Analysis of the Edge Fracture Process in Oscillation for Polystyrene Melts, Rheologica Acta 47 (2008) 929-942.

[53] Q. Huang, O. Hassager, Polymer Liquids Fracture Like Solids, Soft Matter 13 (2017) 3470-3474.

[54] P.A.M. Steeman, J. van Turnhout, Dielectric Properties of Inhomogeneous Media, F. Kremer, A. Schönhals (eds.), Broadband Dielectric Spectroscopy, (Springer, Berlin, 2003), p. 498.

[55] J.A. Puértolas, M. Castro, I. Tellería, A. Alegría, Analysis of the Relaxations on Polymers from the Real Part of a General Complex Susceptibility. Application to Dielectric Relaxations, Journal of Polymer Science Part B: Polymer Physics 37(12) (1999) 1337-1349.

Graphical Abstract